 doi:10.20944/preprints202203.0150.v1

Article

Desert Dust Climatology of Turkey

S. Yeşer Aslanoğlu [1,3,*], Emmanouil Proestakis[2], Antonis Gkikas[2], Gülen Güllü[1] and Vassilis Amiridis[2]

[1] Hacettepe University, Department of Environmental Engineering, Beytepe, 06800, Ankara, Turkey; yaslanoglu@hacettepe.edu.tr; ggullu@hacettepe.edu.tr
[2] National Observatory of Athens, IAASARS, 15236, Athens, Greece; proestakis@noa.gr; agkikas@noa.gr; vamoir@noa.gr
[3] Hacettepe University, Graduate School of Science and Engineering, Beytepe, 06800, Ankara, Turkey; yaslanoglu@hacettepe.edu.tr
[*] Correspondence: yaslanoglu@hacettepe.edu.tr

Abstract: Turkey is located in the heart of complex transition geography between Eurasia and the Middle East. In the grand scheme, the so-called Eastern Mediterranean Basin is almost amidst the dusty belt and a hot spot of climate change. The downstream location of dust carrying winds from the closer desert sources reveals Turkey as an open plane to particulate matter exposure throughout the year. In order to clarify this phenomenon, it is aimed to find out the desert dust climatology of Turkey via CALIPSO onboard Lidar. This prominent instrument enables us to understand clouds, aerosols and their types and relatedly climatic systems with its valuable products. In this study, 9-year CALIPSO derived pure dust product is formed to explain horizontal and vertical distributions, transport heights and case incidences. Results indicated mass and conditional abundancy are higher with the location shifts from west to east. In the same direction, dominant spring months change to summer and autumn. Mountain range systems surrounding Anatolia are the main obstacles against lofted and buoyant dust particles travelling to northern latitudes. Even if high ridges accumulate mass load on the southern slopes, it also enables elevated particles to reach the ground level of the inner cities.

Keywords: aerosol; CALIPSO; desert dust; Eastern Mediterranean; North Africa; Middle East

1. Introduction

Components and their abundancy are consistently changing in water, soil, and air media since the formation of planet Earth. Natural substance flows and corresponding energy balance, namely cycles, are mainly interfered with by direct and indirect human activities. Regardless of human intrusion, natural-originated or anthropogenic substances can be defined as pollutants in the atmosphere due to changes in their abundance. This situation leads to health and environmental quality degradation [1-7]. In order to determine these abundance changes and associated epidemiological and environmental impacts, inventory and climatology studies should be conducted, and prepared outcomes should be kept up to date. By this means, policymakers, environmental, and health authorities can make optimal decisions and undertake affordable risks on local, regional and global scales.

Turkey is located amidst a highly complicated geographical zone since the country constitutes a bridge between the European and Asian mainland next to the African continent. As a result of the intercontinental transition, the most significant part of the country, the Anatolian Peninsula, spreads over the Eastern Mediterranean Basin and the Middle East, the most affected regions of global climate change mid-latitude zone [8-10]. Moreover, surrounding countries and regions have distinctive terrain, flora, and fauna besides societal, industrial, and administrative characteristics. Local contributions of deforested/natural arid regions, mega/medium cities, fossil-fueled power plants, and highly industrialized areas suppress atmospheric conditions. Additionally, this unique crossroad region is under the effect of medium and long-range transport of both biogenic and

 doi:10.20944/preprints202203.0150.v1

anthropogenic pollutants, as described by Lelieveld [11]. Neighboring urbanized, densely populated, and industrialized hot spots, and even political turmoil and armed conflicts in Middle East countries have combined with climate change impacts and led to internal and external intense migration activities. In addition to all these factors, the Anatolian peninsula is amidst of dusty belt and surrounded by two of the largest desert areas in the World (North Africa and the Middle East). According to mid-latitude westerly and local wind patterns, the Middle East and North African deserts originated mineral aerosol, namely dust transport form up an extra load on air quality and relatedly on public health [6,12-14]. This phenomenon also leads to increased expenditures on services provided by central and local authorities such as environmental management, public health, and transportation. Furthermore, within the harmonization process to European Union (EU) acquis, Turkey has obligations to comply with as a candidate country. Within the scope of the Environment Chapter, it is expected that the gradually decreased limit values in the Turkish Environmental Legislation will have to meet stated European levels as of the current year. More clearly, air quality coarse mode particulate matter (PM) concentration limit value has been committed to 50μg/m^3/24hrs and 40μg/m^3/year by 2019. Allowed exceedance for daily limit value is 35 calendar days in a year [15]. Although satellites do not provide aerosol data regarding particulate matter measures based on aerodynamic diameter, guidelines on determining natural contributions to the total load suggest remote sensing, ground measurements, back trajectories, and models [16]. Here, we serve a vision for the 2D and 3D aerosol distributions, specifically desert dust.

Although ground-based in-situ measurements are valuable for assessing air quality variations in urban, rural, and industrial areas, it is impossible to conduct measurements in each desired location. Eulerian and Lagrangian air quality and climate models, specifically space-borne remote sensing instruments, sustain spatiotemporally high-resolution good quality data on the atmosphere and its constituents [17-19].

Over the industrial era, it has been well known that the quantity and the diversity of anthropogenic aerosol types have highly increased in the atmosphere. For overall aerosols, with their direct (-0.27 W/m^2) and indirect (-0.55 W/m^2) radiative forcing effects, which are estimated in recent IPCC reports, the most dominating types are sulfate, black/elemental carbon (BC/EC), and desert dust, respectively [20,21]. Considering the wet and dry deposition mechanism, these moderately long-lived species may have transported and mixed through the Planetary Boundary Layer (PBL) and intra-hemisphere [11]. These full effects still need to be disambiguated to improve effective radiative forcing associated surface temperature alteration estimations. It can be realized via quantifying spatiotemporal variations of anthropogenic and natural aerosol types on regional and global scales [21]. Contrary to relatively younger anthropogenic ones and with inter-hemispheric differences, desert dust is shaping the natural climate cycle via contributing atmospheric cooling, glacier formation, algal bloom, vegetative fertilization, global iron circulation, ice nuclei (IN), and cloud condensation nuclei (CCN) formation and precipitation alterations for hundreds of thousands years [22-27].

The intensity of desert dust outbreaks shows seasonality. Also, dust abundancies may vary from case to case. Due to the geographical location, it is possible to consider the Anatolian peninsula as a 12-month open exposure region to mainly the Middle East and North Africa originated dust advection. There has been a limited number of studies defining dust intrusions to Turkish cities' ambient air for about the last two and a half decades. Early Saharan dust transport studies mainly focus on determining chemical source apportionment of aerosol and rain samples with air parcel trajectories for the Mediterranean region [28-30]. Kubilay et al. [31] firstly stated both the Middle East and North African dust outbreaks within the same methodology perspective with using additional Estimated Time of Arrival (Eta) model and EUMETSAT Meteorological Satellite (Meteosat) visible channel images. Özsoy et al. [32] used the same methodology which previously Kubilay et al. [31] used, with an additional EUMETSAT, Advanced Very High-Resolution Radiometer (AVHRR) visible channel data for describing a hemispheric dust storm in 1994 and discussed the results for Eastern Mediterranean. Kubilay et al. [33] firstly

Preprints (www.preprints.org) | NOT PEER-REVIEWED | Posted: 10 March 2022 doi:10.20944/preprints202203.0150.v1

obtained optical properties of aerosol flux over Mersin, Erdemli with using radiometric measurements at the Institute of Marine Sciences - Middle East Technical University - Erdemli (IMS-METU-Erdemli), NASA, AErosol RObotic NETwork (AERONET) station [34,35]. IMS-METU-Erdemli is the only AERONET station that currently operates in Turkey. However, just one sun-photometer station is insufficient when considering the whole country area, but this substantial station has generated data since the '90s. It has been located at the transport pathway of both North African and Middle East desert areas.

Considering the broader area, including Eastern Mediterranean and the Middle East, it is possible to subclassify dust-related studies into two groups as air quality measurements and remote sensing observations, respectively. In some cases, there are a certain number of studies that use a combination of these techniques in an attempt to empower analysis results. There are pretty several dust-related air quality studies defining the components of PM mass conducted for Anatolian Peninsula [36-38], Cyprus [39], Lebanon [40], Greece [41,42], and broader domain [6] to explain mainly exposure associated health disorders and morbidity. It is possible to extend the list, but the significant point is that in-situ PM measurements may define the mass and, if analyzed, associated physicochemical components at surface elevation, but the proportion of dust intrusion is highly related to mixing height within the PBL. Contrary to the surface and relative to PBL air mass movements, retention time is prolonged if a particle reaches the free troposphere (FT). The particle gains the ability to travel further distances from the source region [25,43]. For this reason, remote sensing observations are quite helpful to clarify columnar atmospheric constituents from ground level up to troposphere or even stratosphere.

In-situ passive instruments (sun-sky-lunar photometers) and Light Imaging, Detection, And Ranging (Lidar)s are prominent tools which are providing aerosol optical characteristics and are used in calibrating/validating space-based sensor data [44]. In addition to columnar passive sensor information [33,45-47], Lidars provide profiling information of atmospheric particles. There are a certain number of Global Atmosphere Watch (GAW), Aerosol Lidar Observation Network (GALION) member networks such as Europe-wide The European Aerosol Research Lidar Network [48] and NASA, Micro-Pulse Lidar Network [49]. Outstanding science groups operate these networks all around the world. These instruments are valuable tools to identify aerosol microphysical properties as systematic and field campaign observations [50-53]. Along with mineralogical alterations [54], optical properties are helpful to identify the differences between dust sources [55]. Apart from ground-based studies, satellite observations have advantageous spatiotemporal coverages. For the last two decades, several research studies have been conducted for the greater Eastern Mediterranean basin utilizing different space-based observation products by most passive instruments. In chronological order of these space-based passive payloads on different satellites are Landsat [56], Meteosat [31,57], Coastal Zone Color Scanner (CZCS) [58], TOMS [45,59], AVHRR [32], METEOSAT Visible and Infra-Red Imager (MVIRI) [58], SeaWİFS [60], Multi-angle Imaging Spectroradiometer (MISR) [61,62], Cloud and Earth's Radiant Energy System (CERES) [62], Advanced Along-Track Scanning Radiometer (AATSR) [63], Moderate Resolution Imaging Spectroradiometer (MODIS) [59,61-63], The Medium Resolution Imaging Spectrometer (MERIS) [58,63], OMI [61,64], Spinning Enhanced Visible and Infrared Imager (SEVIRI) [58], Polarization and Directionality of the Earth's Reflectances (POLDER) [65] used within aerosol related studies in the region. Even though passive space-based instruments provide a high global coverage rate, they fall behind in vertical profiling. Cloud-Aerosol Lidar with Orthogonal Polarization (CALIOP) onboard Cloud-Aerosol Lidar and Infrared Pathfinder Satellite Observation (CALIPSO) satellite is producing 3-D data on aerosol optical properties for more than a decade [66] with a robust identification of mineral dust [67]. Several studies utilized this 3-D dataset in specific dust cases along with a synergistic approach [47,58,68-70] regional scale [64,71] and global scale aerosol or dust research [72-74].

In this study, CALIPSO optimized [75] unique "LIdar climatology of Vertical Aerosol Structure for space-based lidar simulation studies" (LIVAS) [76] pure dust dataset is used to figure out a desert dust climatology over Turkey with surrounding regions. A part of

Preprints (www.preprints.org) | NOT PEER-REVIEWED | Posted: 10 March 2022 doi:10.20944/preprints202203.0150.v1

this dataset (2007 - 2012) was earlier used along with MODIS aerosol and OMI trace gas data by Georgoulias et al. [77] to classify the aerosol types over Eastern Mediterranean (excluding eastern Anatolia). For the first time, Marinou et al. [78] studied the pure dust climatology of Europe, and Proestakis et al. [79] studied south-eastern Asia. This climatology study will be a follow-up of two studies mentioned above and fill a gap for this region (25º - 45º N and 20º - 50º E).

2. Materials and Methods

To compose an aerosol, particularly a desert dust climatology of Turkey, several space-borne remote sensors data are used in this study. They are Cloud-Aerosol Lidar and Infrared Pathfinder Satellite Observation (CALIPSO) onboard Cloud-Aerosol Lidar with Orthogonal Polarization (CALIOP), Aqua onboard Moderate Resolution Imaging Spectroradiometer (MODIS) and Spaceborne Imaging Radar-C/X-Band Synthetic Aperture Radar (SIR-C/X-SAR) derived Shuttle Radar Topography Mission (SRTM3), respectively.

2.1. Study Domain

In order to achieve the main aim, the study domain was selected as comprehensively as possible to cover the whole Eastern Mediterranean Basin and the neighboring dust source regions. Turkey is an intercontinental transition area of the Alpine-Himalayan orogenic belt from Asia to Europe with the Caucasus and Zagros mountains. With climaxes in the Pontic and Taurus ranges, about 15 independently scattered mountains and dormant volcanoes hosting glaciers at an average height of 3.500 m in Anatolia. Mount Ağrı (5.165 m) is the highest dormant volcano with a 10 km^2 ice cap within the region [80]. Conversely to the mountainous structure of Anatolia, there are exciting depression zones located on the broader study domain. The first one is the Dead Sea area (-413 m, Jordan - Israel), the lowest continental region in the World. The others are Qattara (-133 m, Egypt) and the Caspian Sea area (-28 m, Russia - Azerbaijan - Iran, Kazakhstan, and Turkmenistan-not shown here). It is known that these types of depression regions in desert areas pretended as dust transport sources [81,82].

Densely populated cities and sociocultural needs such as shelter, heating/cooling, industrial zones, and transportation networks are significant anthropogenic pollution sources. Eastern Mediterranean basin hosts over 50 moderately big cities as Athens, Baku, and İzmir, seven big cities as Alexandria and Ankara, and two megacities as İstanbul and Cairo [83,84]. Distributed industries, capitals, busy road, rail, air, and maritime transport networks are all included with these crowded settlement zones.

By this means, analysis and the results will be given in the following sections to include the intricate crossover structure of continental and marine bodies of this region. The main study domain and corresponding longitudinal 10º confined three subdomains are depicted in Figure 1. This Digital Elevation Map (DEM) is derived from the SRTM3 Digital Elevation Model [85] so as to reflect the topographic characteristics of the main study domain with its borders.

Climatological horizontal aerosol optical depth (AOD) and pure dust optical depth (DOD) distributions and corresponding temporal behaviors are discussed for the greater study domain in the horizontal distributions section. Climatological and conditional total aerosol, dust, and non-dust cross-sections are examined for the sub-domains in the vertical distributions section.

Preprints (www.preprints.org) | NOT PEER-REVIEWED | Posted: 10 March 2022 doi:10.20944/preprints202203.0150.v1

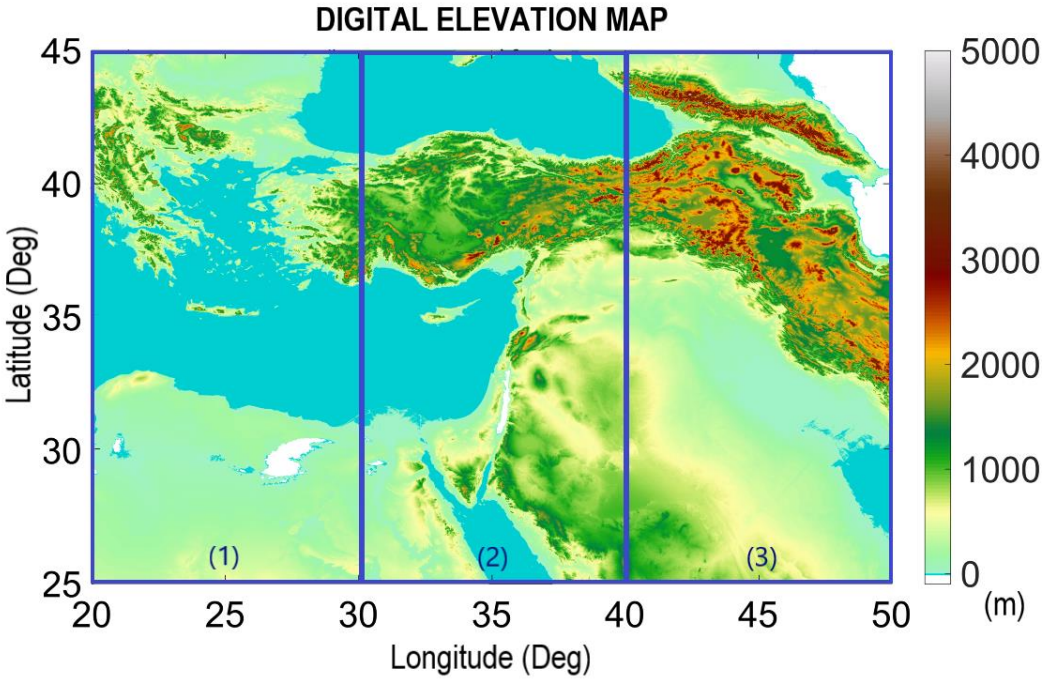

Figure 1. Study domain with corresponding sub-domains: Western 25º - 45º N and 20º - 30º E (**1**), Central 25º - 45º N and 30º - 40º E (**2**), and Eastern 25º - 45º N and 40º - 50º E (**3**).

2.2. CALIPSO - CALIOP

CALIPSO carries out global cloud and aerosol profile observations on a sun-synchronous near-polar orbiting track. Its mission was being a part of NASA's afternoon train (A-Train) constellation and taking simultaneous measurements along with the other member satellites in an ascending mode with equator crossing at around 13.30 local time. In A-Train, CALIPSO arranged its track position regarding Aqua and followed CloudSat's orbital path with a time-lapse of a few seconds. Due to technical problems that affected CloudSat's maneuvering ability in 2017, CloudSat lowered its orbital track as of February 2018. Since they were designed intertwined to achieve sister measurements in the 1990s, CALIPSO started to decline its orbital elevation from 705 km to 688 km in September 2018 to join CloudSat. As of 2018 Autumn, CALIPSO and CloudSat composed a Lidar and Cloud Radar combination of C-Train constellation (capital letter 'C' for each satellite).

CALIPSO has been orbiting around the World since 28.04.2006 with its three onboard payloads. They are NASA and French National Centre for Space Studies (CNES) joint instrument CALIOP, Wide Field Camera (WFC), and The Imaging Infrared Radiometer (IIR). CALIOP, the nadir pointing polarization Lidar instrument, provides high resolution attenuated backscatter profiles from the polarized laser channels of 1064 nm and 532 nm. Horizontally 333 m (at along-track) and vertically 30 m (up to 40 km) resolution meets in nanoseconds above clouds, below thin clouds, and clear sky conditions [66,86].

CALIPSO processing algorithm detects the vertical location of each atmospheric layer [87], discriminates clouds from aerosols [72], and then classifies aerosol layers into sub-types as dust, polluted dust, marine, continental, and clean continental. The last and the most significant step is in this classification process is using Lidar Ratio (LR) values which are predicted according to extinction (σ) to backscatter (β) ratio for each sub-type. More detailed data optimization is made by utilizing ground-based EARLINET stations, and also data validation is made by using the data of globally distributed stations of the AERONET network [67,75,76].

In this study, CALIPSO Level 2 (L2), Version 3 (V3), horizontally 2º×5º resolution data are used to derive 1º×1º resolution pure desert dust aerosols and associated conditional and climatological distributions. The study time window between 01.01.2007 and 31.12.2015 pertains to the A-Train constellation period. Moreover, this data does not

Preprints (www.preprints.org) | NOT PEER-REVIEWED | Posted: 10 March 2022 doi:10.20944/preprints202203.0150.v1

belong to the laser degradation anomaly period from 01.09.2016 up to the present. This low-energy anomaly reveals the decreasing quality of laser shots and the related products. Anomaly period can be used with a strict filtering process, but this study intends not to interfere with climatological data uniformity process procedures of EARLINET methodology.

To derive pure dust product, the discrimination methodology of Lidar climatology of Vertical Aerosol Structure for space-based lidar simulation studies (LIVAS) database is implemented to the dataset [76]. EARLINET and European Space Agency (ESA) joint product of LIVAS database produce quality ensured, cloud screened, EARLINET optimized. AERONET evaluated data described in more detail by Amiridis et al. [75] together with the filtering procedure recommended by Winker et al. [66]. Moreover, dust and polluted dust sub-types processed once again to gather pure dust σ product are calculated according to CALIPSO polluted dust and dust subtypes [75].

About 30 thousand, 5 km nominal resolution profile and layer files are downloaded from Cloud-Aerosol-Water-Radiation Interactions (ICARE) Data and Archive Center (http://www.icare.univ-lille1.fr/archive) to implement the aforementioned depolarization-based discrimination method of EARLINET. Downloaded data is sub-setted to polarization-sensitive 532 nm, the most suitable window for dust, and georeferenced to the selected study domain. Both profile and layer files include geolocation, time, Cloud-Aerosol-Discrimination (CAD) Scores, corresponding uncertainties, and quality descriptive flags. Besides that, profile files include perpendicular and parallel optical depth, extinction and backscatter coefficients, particle depolarization profiles, and surface elevation statistics. On the other hand, layer files include surface feature properties, parallel and perpendicular column optical properties, extinction and backscatter coefficients, and particle and volume depolarization ratios (δp).

Shifting LR values is an advanced step to retrieve desired products from the global dataset. LR is set to the current announced global dust value as 44 sr [88]. However, 55 ± 7 sr is representative for Saharan dust and 43 ± 5 for the Middle East [89-91]. Nevertheless, Turkey is affected by dust transport from mostly Saharan, the Middle East, and rarely Asian deserts [92]. Moreover, the study domain partially includes these source regions themselves. These arguments make 44 sr LR value the most suitable for our region.

Following the procedure steps, other strict cloud features, and quality screening procedures, this data set has 30 - 160% uncertainties for extinction coefficient and 30 - 100% for AOD [78]. According to the CALIPSO raw data release and error analysis report, random error propagation results have no vital defects [93]. Data is at acceptable limits, and the bias values are negligible. A detailed explanation of the methodology and European implementation of this data can be found at Marinou et al. [78], and also Asia implementation can be found at Proestakis et al. [79].

2.3. Aqua - MODIS

Aqua is one of the triplet satellites (Aqua, Aura, and Terra) of NASA, a significant member of the A-Train satellite constellation since 04.05.2002. For the time window of this climatology study, Aqua and CALIPSO had the same orbital track with a small-time gap that Aqua was 0.2 min faster than CALIPSO. Naturally, these time differences allow collecting data from payloads following the same orbital track. At 705 km above the ground, synchronous near-polar orbiting Aqua has several payloads at cross-purposes onboard. These instruments are Atmospheric Infrared Sounder (AIRS), AMSU-A, Humidity Sounder for Brazil (HSB), Advanced Microwave Scanning Radiometer for EOS (AMSR-E), CERES, and MODIS.

In order to have a confidential reference point for the total aerosol, MODIS data is used to compare CALIPSO aerosol and associated products. Since Lidar and Spectroradiometer have different specifications, observations differ from each other. Whereas passive instruments have some challenges in discriminating aerosol properties in path radiance with an interfering effect of Top of Atmosphere (TOA) radiance. Since TOA radiance

Preprints (www.preprints.org) | NOT PEER-REVIEWED | Posted: 10 March 2022 doi:10.20944/preprints202203.0150.v1

includes earthshine spectra, as a first step, path radiance should be separated from the observation with specific assumptions. Same as the way that other passive instrument methodologies have, MODIS is using a theoretical model and additionally SeaWiFS observations in recently updated aerosol algorithms. MODIS has a particle size-based aerosol typing method whose products are used to compare CALIPSO derived products on a horizontal 2D basis.

The across-track scanning radiometer MODIS has higher spatiotemporal coverage than CALIOP. It has a 7,085 km swath width and temporally covers the world within 1,5 days, while nadir pointing CALIPSO needs 16 days. MODIS utilizes solar energy with 36 spectral bands (0.4 - 14.5 μm) as a passive sensor to carry out Earth observations.

To gather aerosol information for comparing patterns with CALIPSO derived pure dust product, MODIS daily 1º×1º resolution, Collection 6, L3 MYD08-D3 global atmosphere products are used in this study. Although the collection is updated to its recent version of 6.1, it is suitable to use Collection 6 to follow the A-Train period of CALIPSO. Moreover, the 550 nm dataset, within the convenient spectral window for dust, was validated over a part of the Eastern Mediterranean Basin previously [94]. There are two algorithm types that the MODIS science team uses to retrieve atmospheric profile, stability parameters, water vapor, optical and physical properties of aerosols and clouds, ozone abundancy. The first one of these algorithms is Dark Target (DT), specifically for dark surface features. The other is the bright surface-specific Deep Blue (DB) algorithm [95]. In this study, a gridded and cloud screened DT & DB combined product covers whole columnar measurements over both continental and ocean surfaces. MODIS datasets are available at NASA Atmosphere Archive & Distribution System (LAADS) website (https://ladsweb.modaps.eosdis.nasa.gov/) via Distributed Active Archive Center (DAAC).

2.4. Trend Decomposition Analysis

Horizontal pure dust data of western, central, and eastern domains were statistically analyzed via Seasonal and Trend Decomposition using Loess (STL) method [96]. This robustly decompose a given time series data into seasonal, trend, and residual components using embedded Loess regression curve smoothing with ordinary least squares polynomial fit. There are six main steps in this method: 1. de-trending, 2. smoothing of cycle subseries, 3. filtering of smoothed cycle subseries, 4. de-trending of cycle subseries, 5. deseasonalizing, and 6. trend smoothing, respectively. At the end of these statistical steps, basically, primary time-series data (Y_t) can be decomposed into seasonal cycle (S_t), trend-cycle (T_t), and residuals (R_t) as Equation 1 shown below.

$$Y_t = S_t + T_t + R_t \quad (1)$$

3. Results and Discussion

3.1. Horizontal Distributions

In this part of the results section, CALIPSO derived total, and seasonal mean aerosol optical depth (AOD), and pure dust optical depth (DOD) horizontal distributions are presented for the period between 01/01/2007 and 31/12/2015. Horizontal outputs are plotted with 1º×1º spatial resolution CALIPSO derived product for the wider domain (20º - 50º E and 25º - 45º N) to indicate climatological distributions. 9-year AOD and DOD mean values and their ratio are depicted in Figure 2 for the entire time window. As for the total domain, the mean AOD value is 0.20±0.04, significantly increasing in eastern longitudes where the Mediterranean Sea ends and Middle East desert areas start to exist longing to the Persian Gulf. The region includes some of the world's most crowded cities as Athens, İstanbul, İzmir, Ankara, and Cairo. Also, it spreads to the southeastern shores of the Caspian Sea together with the Eastern part of the Mediterranean Sea and the Black Sea, which reveals anthropogenic and marine aerosol contribution to the total AOD load. Cairo and most parts of Iraq, Kuwait, Saudi Arabia, and Iran have the highest AOD values in the

Preprints (www.preprints.org) | NOT PEER-REVIEWED | Posted: 10 March 2022 doi:10.20944/preprints202203.0150.v1

region as 0.43 and 0.61, respectively. If we approach the region in terms of desert dust, Mega-City Cairo [84] differs from the Eastern side of the Red Sea with about 60 % of anthropogenic and marine aerosols. The Middle East part or the main domain has 70 – 100 % dust abundance in the total aerosol budget. Decreasing values down to 0.05 can be observed in northern longitudes over the Black Sea, highly forestry and mountainous northeastern Anatolia, and the Caucasus region (~3.5 - 4.5 km), which have endemic flora, fauna and exceptionally high oxygen levels, and a few specific parts of the Aegean Sea and inner Anatolia. The mountainous structure of this territory can also be tracked from the Digital Elevation Map (DEM) depicted in Figure 1.

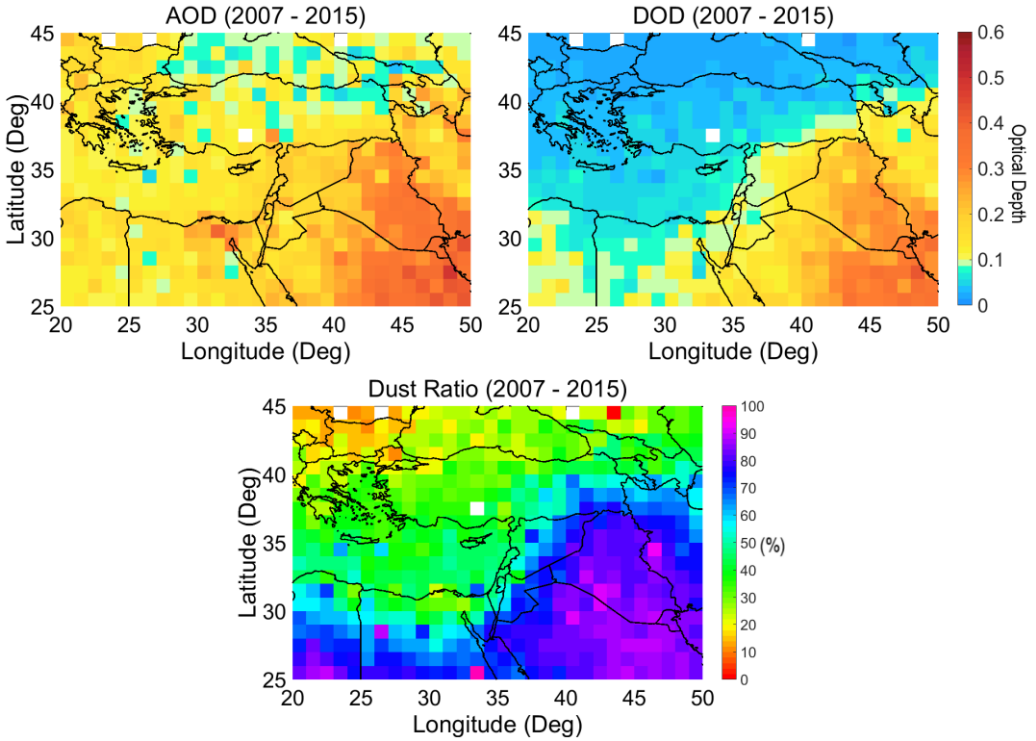

Figure 2. Total 9-year horizontal aerosol & pure dust distributions with corresponding pure dust to total aerosol ratio.

The average Pure Dust Optical Depth (DOD) value for the whole domain is 0.10±0.02, increasing in desert areas with an apparent peak of 0.42 around the Persian Gulf. The mean DOD value over Anatolia is ~0.05 with a significant increase up to 0.1 in the southeastern part of Turkey close to source regions at the Syria, Iraq, and Iran border. Further cities from the Mediterranean Sea shoreline as Şırnak and Hakkari, dust pattern seems like an extension of the Middle East source. Highly industrialized zone of the Marmara and Aegean (western) parts including megacity Istanbul, additional Çukurova (last shores of east Mediterranean at Turkey) with numerous large installed capacity thermal power plants and harbors, capital Ankara and arid regions of Konya - Karaman basin (at south of Ankara) indicates the non-dust aerosol contribution to total load. The pure dust to total aerosol ratios of Marmara, Aegean Sea, Çukurova, and Konya-Karaman basin are ~20 %, ~25 %, ~40 %, and ~30 %, respectively.

It is possible to emphasize anthropogenic aerosols in these areas, including continental dust impact around Tuz Lake on Konya - Karaman basin. As depicted in Figure 1, ridge elevations are lower in the Aegean and Marmara coasts, penetrating plains to inner Anatolia, which carries marine climate further away from the water body. However, this study does not contain any other aerosol type. Specifically, it is possible to mention marine aerosols in plain coastal regions. Also, the alluvial plain of Adana, similar to Antalya on the Mediterranean coast, enables us to refer to marine aerosol contribution in these areas; likewise, the other countries have the Mediterranean and the Black Sea coastlines.

 doi:10.20944/preprints202203.0150.v1

A primary synoptic, seasonal classification in simplest terms as winter (December-January-February-March), spring (April-May), summer (June-July-August-September), and autumn (October-November) was made by Alpert et al. [97]. This classification clarifies the systems carrying dusty winds to the Eastern Mediterranean Basin. In the winter wet season, westerlies generated over Italian Alpines dominate the region with high sea surface temperature, causing low troughs and precipitation blocking Red Sea troughs [98]. Also, southwesterly Lodos is affecting the Aegean Sea environment. In spring, Khamsin (Sharav) low dominates the region with dry heat strokes for about 50 days as the meaning of Arabic wording Khamsin. Except for the Khamsin days period, the Red Sea trough is adequate this season. In the summer months, the western branch of the Asian Monsoon, Persian troughs is effectual over Anatolia, reaching Aegean costs and subtropical highs [99]. Conversely, to Lodos, Etesian (Meltemi) winds reach Egypt from the Aegean Sea [100]. In their classification's autumn, the Persian trough starts to decay and leaves the region to the Red Sea troughs [97]. According to these synoptically classified seasons, it is evident that dust-carrying winds are arriving over Anatolian land throughout the year.

In this study, out of those synoptic-based seasonal classifications mentioned above, 3-month seasonal grouping for 9-year DOD distributions is organized as November-December-January (NDJ), February-March-April (FMA), May-June-July (MJJ), and August-September-October (ASO) based on monthly mean distributions (108 months, not shown here) and also 9-year monthly mean distributions depicted in Figure A1. Seasonal grouping starts with the first observed particular dust transport pattern in February. As solar irradiance starts to increase at the end of the cold-wet months on the Eastern Mediterranean basin, dust particles become lofted with the prevailing winds from both Sahara and the Middle East deserts, apparently as shown in Figure A1 and Table 1. According to this seasonal grouping, the ratio of dusty overpasses, DOD, and AOD values of CALIPSO are presented in Figure A2. Based on these maps, it is possible to notice 0 % dusty pixels in the Caucasus part in FMA and NDJ seasons. Once the dust particles are suspended from the surface and gain head, they can travel long distances. Also, over the climaxes of Turkey in the eastern region, values decrease dramatically by 10 %. This drop can be explained by the sudden elevation increase there (Figure 1); the high ridges form a natural barrier against dust transport. However, data is generally of good quality in all seasons with an average 70 % dust occurrence score (Figure A2). 100% values naturally observed over closer sources of the Middle East.

1º×1º confined, and seasonally classified 9-year mean CALIPSO Pure Dust Optical Depth (DOD) and Aerosol Optical Depth (AOD) horizontal distributions are depicted in Figure 3 together with concurrent MODIS AOD distributions. For the same seasonal classification Dust Center Height (DCH, km) and Dust Top Height (DTH, km) views are depicted in Figure 4. Additionally, seasonal summary statistics on AOD, DOD, DCH, and DTH are given in Table 1. Since MODIS quality ensured atmospheric products are broadly used and mostly validated, it is a good reference point to compare with CALIPSO derived products of this study. The same procedure and time window are used for MODIS AOD data as retrieved, geographically confined, and seasonally classified. Correlations between MODIS AOD and CALIPSO DOD and AOD results are very high at the level of 95-97 % except for the Western part. In general, CALIPSO observations tend to have lower values than MODIS from the nature of its remote sensing technique. While the passive sensor onboard Aqua has a large swath width (> 700 km) on the Earth's surface, CALIOP has only laser shot points in an orbital row. In the present case, measurement density is inherently low, as it is impossible to mention the instantaneous horizontal coverage for the onboard Lidar. This lower measurement density becomes apparent in the Western subdomain. In this region, dust and aerosol abundancy is rare with respect to the neighboring and the Eastern part. Lower abundancy causes lower AOD and accordingly causes lower correlation with MODIS AOD (89 % in West).

Preprints (www.preprints.org) | NOT PEER-REVIEWED | Posted: 10 March 2022 doi:10.20944/preprints202203.0150.v1

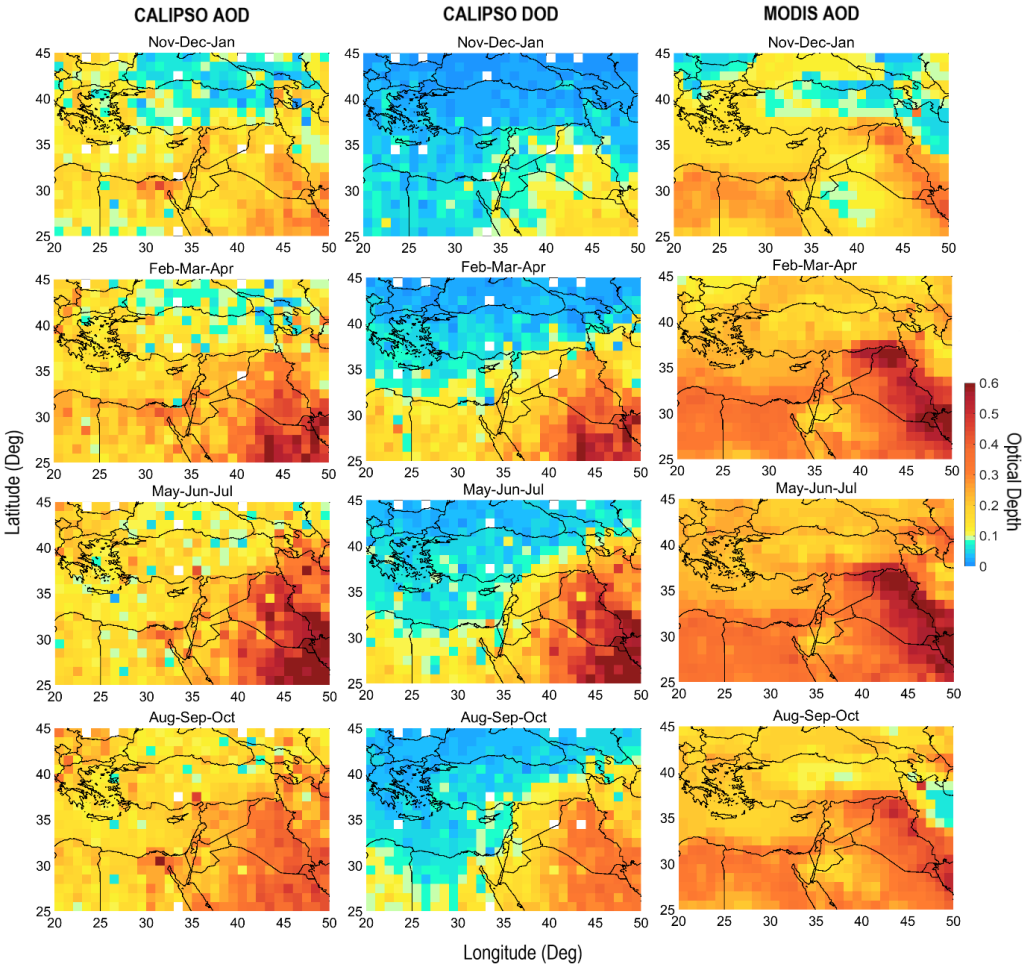

Figure 3. 9-year seasonal CALIPSO total aerosol, CALIPSO derived pure dust & MODIS total aerosol horizontal distributions.

At first glance from Figure 3 and the monthly distributions in corresponding Figure A1, it is possible to classify NDJ as low, FMA as transition, and MJJ and ASO as high dust-affected seasons for Anatolia. Dust patterns increase in FMA concerning NDJ and decrease in ASO relative to MJJ. Especially over the Mediterranean shores of North Africa, dust starts to become lofted (Figure 4) and transported to remote locations from the sources due to the prevailing wind characteristics. As the wet season comes to an end, solar energy intensity increases, and the transition process to spring season begins. In February, dust-carrying Lodos winds begin to gust through upcountry and reach even the Black Sea. However, Lodos winds turn out to be storms with an average speed of 80 km/h over the Aegean Sea, Çanakkale (Dardanelles) Strait, Marmara Sea, and Bosporus (İstanbul). Following this, soil moisture and humidity decrease over source regions [101] accordingly, dust particles reach to top levels in the troposphere (~6 km), and dust abundance increase to maximum values (~2.5) in FMA season throughout the basin.

Figure 3, Figure 4, and Table 1 show that the highest season in terms of all parameters is MJJ. Dust is the significant contributor to total aerosol load in these months, and it apparently shows an ascending trend. Parallel to increased mass loading, transport elevations are rising to the climaxes of the mountain ranges from the Zagros to the Caucasus. From this point of view, transport heights of dust particles are quite different compared to other seasons. The center of the peak mass loading in an atmospheric measurement column, DCH in our case, is elevated parallel to DTH. This reveals dust particles overcome high obstacles of the Taurus, North Anatolian, and Caucasus mountain ranges. Thus, dust plumes reach the most remote places in the back slopes of ridges and tend to dry deposit.

Preprints (www.preprints.org) | NOT PEER-REVIEWED | Posted: 10 March 2022 doi:10.20944/preprints202203.0150.v1

In ASO season, although transport elevations are slightly decreasing concerning MJJ, still lofted particles have the ability to climb over high ridges. Conversely to the FMA season, the solar intensity falls from the second half of August. Hot spots over the Middle East and North Africa are getting smoother in proportion to the previous warm months, and the dust pattern recedes to low latitudes. As the season turns out to be Autumn, precipitation causes particulate matter scavenging from the atmosphere. Secondly, particles faced with high mountain ranges with a decreased vertical head tend to accumulate in the front slopes more than that of the back slopes of the climaxes.

Table 1. Summary statistics of 9-year seasonal DOD, max. DOD, dust to the total aerosol ratio (DR, %), dust center height (DCH, km), dust top height (DTH, km) for the broader and the individual subdomains.

	Season	DOD ± Std	Max. DOD	DR (%)	DCH ± Std	Min. DCH	DTH ± Std	Max. DTH
Broader Domain 25º - 45º N and 20º - 50º E	NDJ	0.05 ± 0.08	1.35	38.36	1.40 ± 0.51	0.37	2.29 ± 0.57	4.12
	FMA	0.12 ± 0.19	2.47	66.58	1.86 ± 0.53	0.44	3.18 ± 0.68	5.85
	MJJ	0.14 ± 0.20	2.58	71.22	2.01 ± 0.53	0.82	3.58 ± 0.76	5.73
	ASO	0.10 ± 0.13	1.79	55.47	1.81 ± 0.59	0.54	3.25± 0.81	5.61
Western (1) 25º - 45º N and 20º - 30º E	NDJ	0.03 ± 0.06	0.81	29.94	1.23 ± 0.40	0.47	2.07 ± 0.51	3.97
	FMA	0.08 ± 0.12	2.47	51.88	1.69 ± 0.37	0.70	2.91 ± 0.56	5.59
	MJJ	0.07 ± 0.08	1.02	50.16	1.74 ± 0.36	0.82	3.09 ± 0.48	4.34
	ASO	0.05 ± 0.06	0.88	35.37	1.45 ± 0.30	0.61	2.65 ± 0.39	4.35
Central (2) 25º - 45º N and 30º - 40º E	NDJ	0.05 ± 0.07	0.69	38.32	1.37 ± 0.44	0.37	2.25 ± 0.49	3.78
	FMA	0.09 ± 0.14	1.67	59.67	1.84 ± 0.52	0.44	3.11 ± 0.64	5.07
	MJJ	0.09 ± 0.12	1.70	59.29	1.91 ± 0.48	0.96	3.38 ± 0.63	4.95
	ASO	0.08 ± 0.10	1.79	48.94	1.74 ± 0.52	0.54	3.11 ± 0.70	4.99
Eastern (3) 25º - 45º N and 40º - 50º E	NDJ	0.07 ± 0.10	1.35	44.94	1.59 ± 0.63	0.50	2.54 ± 0.63	4.12
	FMA	0.20 ± 0.25	2.13	80.19	2.06 ± 0.63	0.71	3.51 ± 0.71	5.85
	MJJ	0.27 ± 0.27	2.58	85.96	2.37 ± 0.52	1.49	4.28 ± 0.60	5.73
	ASO	0.18 ± 0.16	1.76	71.98	2.23 ± 0.61	1.23	3.98 ± 0.66	5.61

With the month of November, autumn transition completed and leaves its mission to cold-wet weather conditions. Dry deposition leaves its place to scavenging systems via snow and rainfall. Numerous scientific groups have studied atmospheric dust contribution to CCN and IN formation mechanisms [22-27, 102]. As NDJ is defined as the low season, in November, the frequency of Lodos storms is getting lower, but wind speed is increasing dramatically. The most recent extreme event had reached up to 150 km/h over İstanbul. Dust is bringing precipitation, and scavenging drops the dust in the air, vice versa [103].

Preprints (www.preprints.org) | NOT PEER-REVIEWED | Posted: 10 March 2022 doi:10.20944/preprints202203.0150.v1

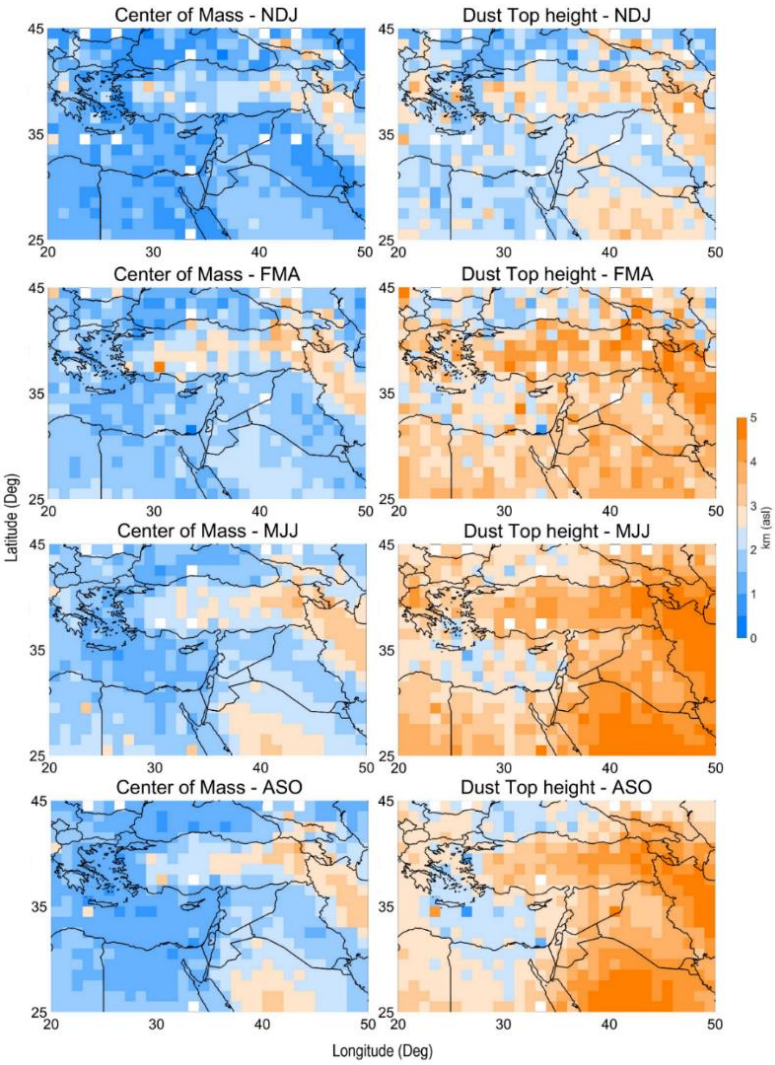

Figure 4. 9-year seasonal mean dust center height (mass, DCH) & dust (mass, DTH) top height horizontal distributions (asl-km).

Out of monthly synoptic variations, massive oceanic oscillation systems regulate the inter-annual changes in dust fluxes in the atmosphere. The area between Euphrates and Tigris rivers in The Middle East is called Fertile Crescent. It is almost wholly a desert without the presence of water. Synergistic effects of Pacific Decadal Oscillation (PDO) and El Niño Southern Oscillation (ENSO) are mainly responsible for precipitation drops and, accordingly, droughts in the region [101]. It is well known that the North Atlantic Oscillation (NAO) has a significant impact on Saharan dust mobility [104].

Trend decomposition analysis is conducted for 9-year (108 months) pure dust data derived from the CALIPSO product. Analysis results are depicted as a regional (year^{-1}) map and relevant trends in Figure 5. The significance of the analysis results are primarily between 90-95 % confidence interval, and seasonally decomposed trends tend to decrease slightly in all three domains. Especially there is an increasing pattern after 2007, which is the most affected year from the oscillation dynamics in the Middle East. As the soil moisture descends, dust mobility ascends [104]. It is possible to describe all three sub-domains are matching and nonmatching in certain points. There is a highlighting peak in the middle of 2011 in the Central and Western parts. Before 2011, it is smoother and lower in Central concerning Western and Eastern. There are two peaks till 2012 in the West, but the trend is more continuous and inflated in the East, with a significant peak closer to the beginning of 2011, not in the middle. However, the mass load increased from the West to the East; another critical point was the decrease in 2014. It can be attributed to the increase

Preprints (www.preprints.org) | NOT PEER-REVIEWED | Posted: 10 March 2022 doi:10.20944/preprints202203.0150.v1

in precipitation and soil moisture experienced in the same year. The correlation between soil moisture, precipitation, surface wind and AOD in The Middle East is described by Klingmüller et al. [101]. In that study, MODIS-AOD trends were calculated based on two different time windows as 2000 – 2015 and 2001 – 2012, respectively. For those periods, it has been found out that there is a strong increasing trend (within 99 % confidence interval) for mainly the Arabian Peninsula in that study. It should be pointed out that the total aerosol load may cover all natural and anthropogenic particles for the observed region. Here, pure dust trends of this Eastern Mediterranean domain is calculated for the first time, and decreasing trends are mainly located below the southern Turkish border. Parallel findings of sand and dust (SDS) observations reveal a descending lofted dust mass between the southern Turkish border and the north-western side of the Persian Gulf [105].

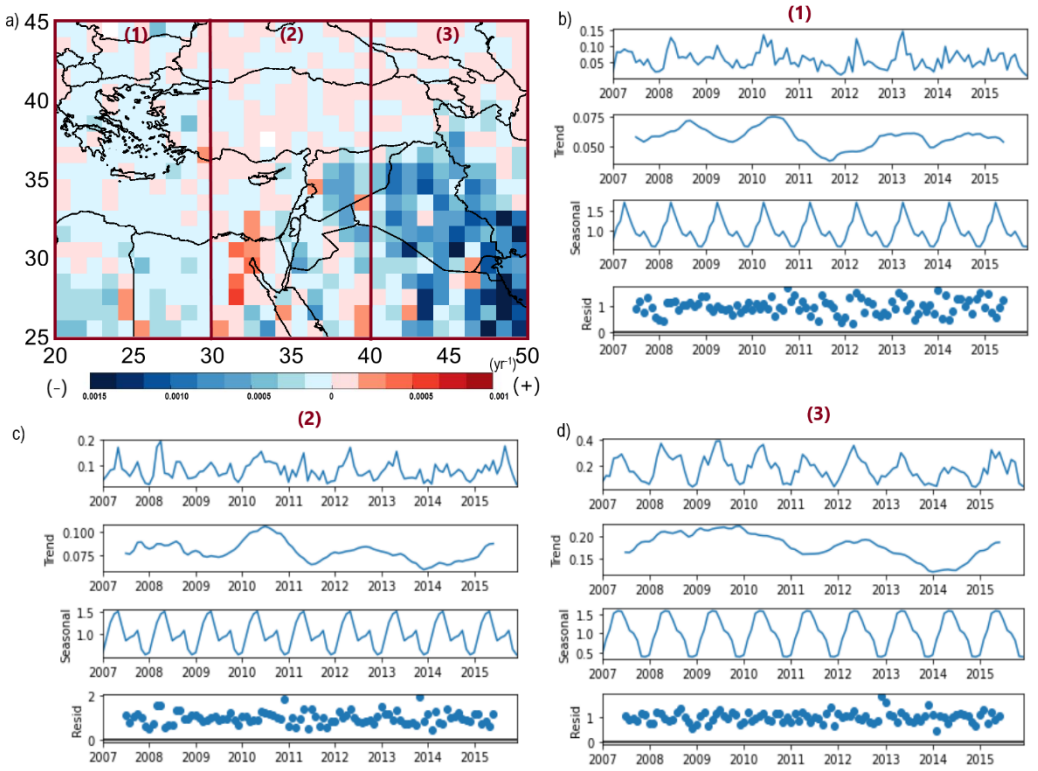

Figure 5. 9-year (108 months) trend slopes for main and corresponding subdomains (**a**); trend, seasonality and residue decomposition for sub-domains: (**b**) Eastern, (**c**) Central, and (**d**) Western.

3.2. Vertical Distributions

3.2.1. Climatological Profiles

Climatological extinction cross sections for total, dust and non-dust aerosols are presented for the three sub-domains in this part. Within the broader domain, longitudinal 10º confined sub-domains are previously given in Figure 1. The same seasonal grouping gathers longitudinally averaged vertical profiles up to 10 km above mean sea level. Following cross-sectional maps also include embedded minimum, average, and maximum mean elevation information for the 10º slices.

Horizontal optical depth turns out to be columnar extinction on a vertical basis. From a different point of view, extinction cross-sections of total, dust and non-dust aerosols are decomposed for the Western sub-domain between 20º - 30º E and 25º - 45º N are given in Figure 6. This part includes highly industrialized and densely populated west Anatolia and Marmara regions with Greece, Macedonia, Bulgaria, and partially Albania, Serbia, Romania, Libya, and Egypt. Slight depression, namely source zones in Libya and the significant Qattara region in Egypt, are located herein. The lowest transport elevations and corresponding low values for all types are observed here, considering the other two sub-

Preprints (www.preprints.org) | NOT PEER-REVIEWED | Posted: 10 March 2022 doi:10.20944/preprints202203.0150.v1

domains, which are also mentioned in horizontal distributions. Lodos is effective in the wet season while Khamsin winds in the dry season. Also, Khamsin winds are the critically responsible for high temperatures and drying soil in the broader Eastern Mediterranean Basin. By the Lodos and prevailing westerlies gusting through the Aegean Sea up to the northern areas, pure dust values increase in FMA season. The pure dust portion in the total load is dramatically increasing with the lofted particles from the source regions. It becomes evident between 25º - 35º N until the buoyant particles face the Taurus mountain range barrier. Additionally, by the Persian through, which is the western part of the Asian Monsoon, transport heights are kept more or less identical in MJJ for the previous months. When summer starts to shift autumn, both elevations and abundance show an attenuated profile conversely to the inclining non-dust aerosols between 35º - 45º N.

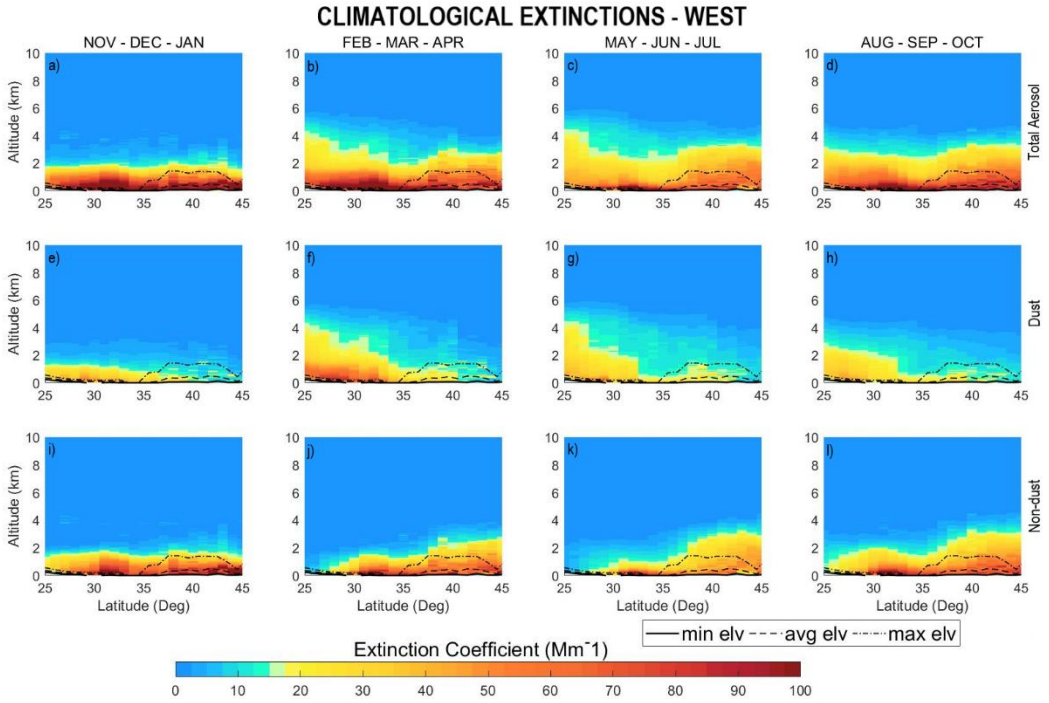

Figure 6. Climatological vertical total aerosol (**a-d**), pure dust (**e-h**) & non-dust aerosol (**i-l**) seasonal distributions of the Western subdomain with corresponding topographic information. Seasons: (**a,i,l**) NDJ, (**b,f,j**) FMA, (**c,g,k**) MJJ, and (**d,h,l**) ASO.

Especially it is possible to emphasize that from mid to northern latitudes, the non-dust part with a marine portion is specifically dominated by anthropogenic aerosols in total aerosol load. Highest season FMA in the western domain shifts to summer months as we move to the east. Figure 7 depicts the climatological seasonal vertical dust cross sections for the Central sub-domain between 30º - 40º E and 25º - 45º N. It covers central Anatolia, the Sinai Peninsula, the Red Sea, and the Middle East countries in the Mediterranean basin. This sub-domain has higher values than the western one is highly connected with those mentioned earlier dust-carrying synoptic systems. Besides westerlies and Khamsin low, the Persian trough and the Red Sea trough are more effective. Persian trough shifts peak values effectively to MJJ and ASO seasons. From 35º N latitudes of Anatolia, because of the increasing average elevations with continuing Taurus system, abundancy of transported dust increases in ground levels. Accumulation due to the downslope effect leads to air quality degradation in the southern slopes of the seashore. Also, other types of aerosol, which can be a mixture of continental and anthropogenic, are highly abundant in the other direction of the downslopes. However, it can be seen that the dust particles which could pass through the topographical barrier they encountered and reach mid-Anatolia at ground level. Another crucial barrier against the northern latitudes is that the Black Sea mountain ranges stand between the mainland and the sea.

Preprints (www.preprints.org) | NOT PEER-REVIEWED | Posted: 10 March 2022 doi:10.20944/preprints202203.0150.v1

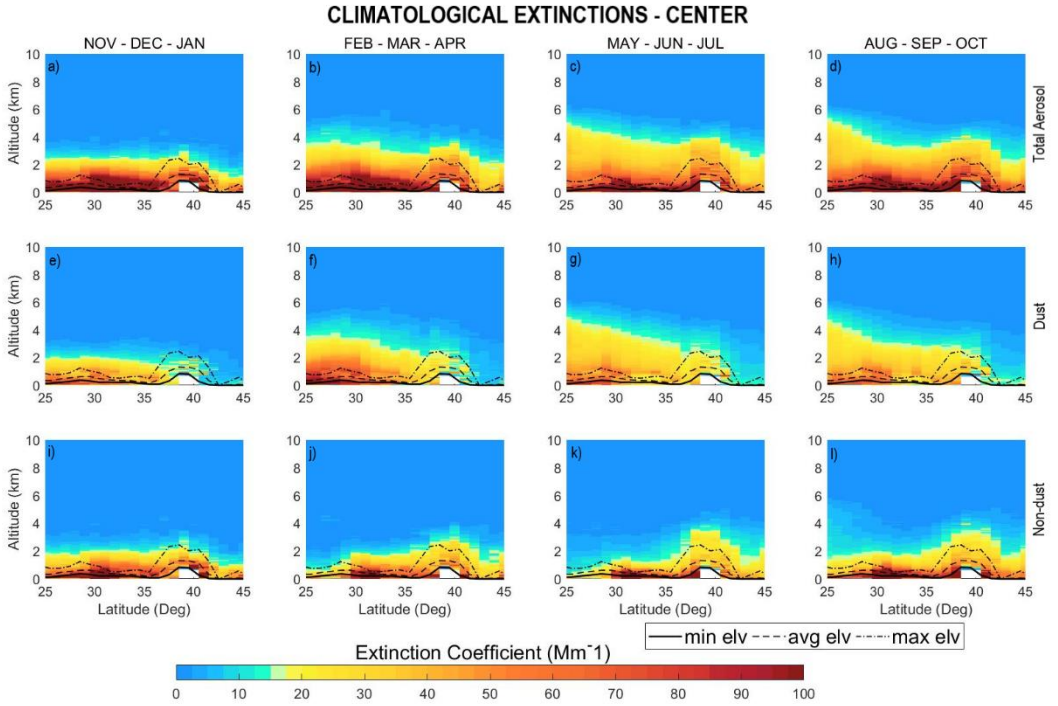

Figure 7. Climatological vertical total aerosol (**a-d**), pure dust (**e-h**) & non-dust aerosol (**i-l**) seasonal distributions of the Central subdomain with corresponding topographic information. Seasons: (**a,i,l**) NDJ, (**b,f,j**) FMA, (**c,g,k**) MJJ, and (**d,h,l**) ASO.

Climatological seasonal total, dust, and non-dust cross sections for the eastern subdomain between 40º - 50º E and 25º - 45º N are depicted in Figure 8. Besides 3.000 m average elevations, altitude drops dramatically towards the Middle East in the southeastern part of Turkey. Close by Dead Sea shores, topography changes dramatically to below mean sea level reveals to depression zones that are probable source regions. A significant part of the Middle East countries and the northern shores of the Persian Gulf is located herein. Large dust source areas are also located in this sub-domain, even with a direct continental connection without the buffer of the mountain ranges surrounding the Mediterranean Sea. Southeastern mean sea level planes penetrate the inner parts as the Taurus mountain range edge out to the northern latitudes. It is possible to characterize this region as the most different in terms of general aerosol density, dust density, transport height and topography variance. Even the FMA season, which has the lowest intensity, has many times higher values than the seasons with the highest intensity in other regions. It can be attributed to the northern hemisphere's dominating wind types on a diagonal axis from the southwest to northeast comes from the curvature and the orbital direction of the globe. A wide range of transported dust can meet the region whether it is only Saharan or Middle East dust or is a mixture of both. It is known that there is also transport from the desert regions of near Asia, although it is very infrequent [92]. Since the transport heights are too high, the Eastern Anatolian mountain ranges do not always form an obstacle against the dust. However, the Caucasus Mountains do not allow dust to pass to higher latitudes as a second obstacle. MJJ and ASO seasons show similarities in dust heights, but in terms of intensity, FMA and MJJ seasons are more similar at lower altitudes. Non-dust intensity at lower altitudes increases in NDJ, most probably due to heating purposes for this mountainous region. It is possible to interpret local, continental dust contribution for deforested areas. In some cases, dust devils and haboobs can be experienced in the southern areas of Turkey [106], just as in the Konya-Karaman basin in Central Anatolia.

Preprints (www.preprints.org) | NOT PEER-REVIEWED | Posted: 10 March 2022 doi:10.20944/preprints202203.0150.v1

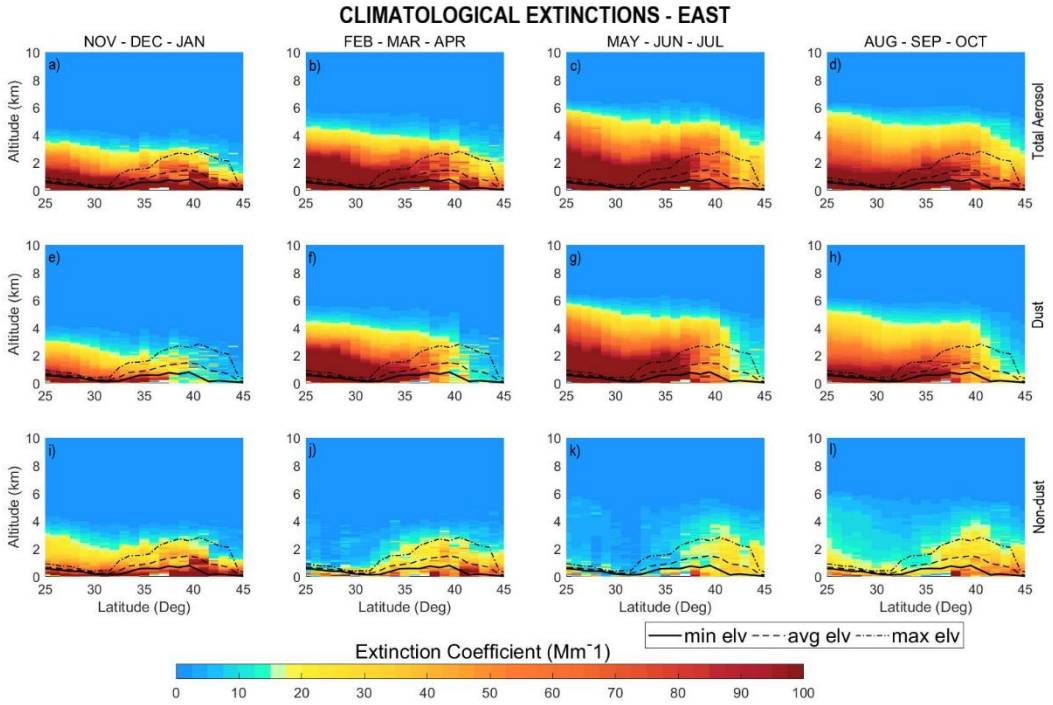

Figure 8. Seasonal climatological vertical total aerosol (**a-d**), pure dust (**e-h**) & non-dust aerosol (**i-l**) seasonal distributions of the Eastern subdomain with corresponding topographic information. Seasons: (**a,i,l**) NDJ, (**b,f,j**) FMA, (**c,g,k**) MJJ, and (**d,h,l**) ASO.

3.2.2. Conditional Profiles

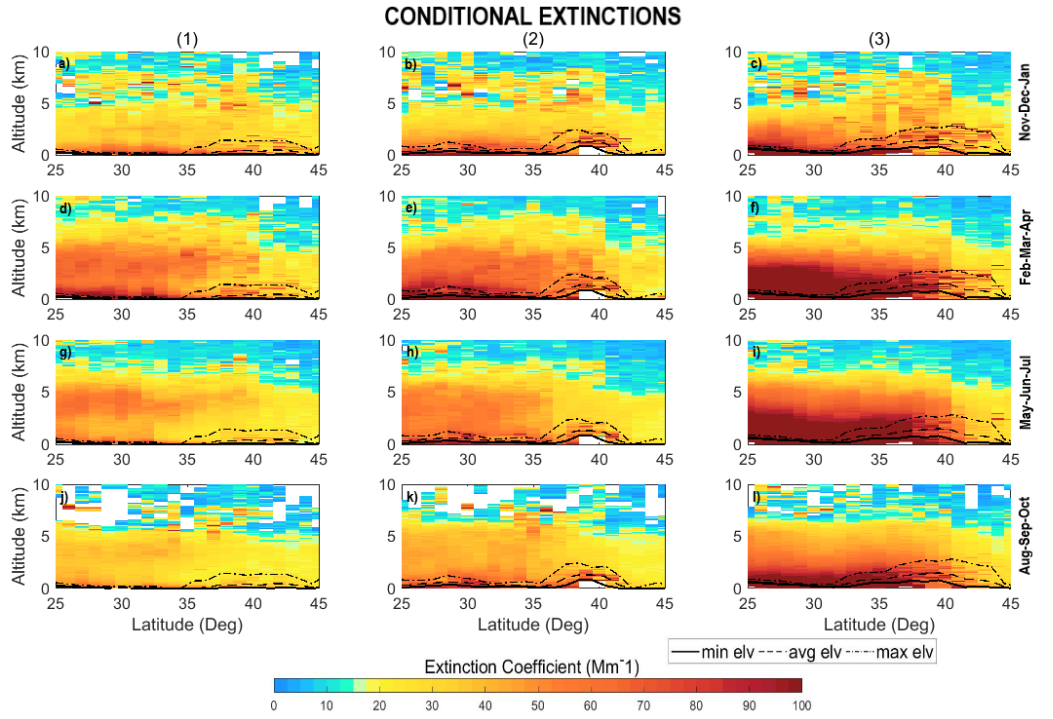

Figure 9. Seasonal conditional vertical pure dust distributions of (**1**) Western: (**a,d,g,j**), (**2**) Central (**b,e,h,k**) & (**3**) Eastern (**c,f,i,l**) subdomains with corresponding topographic information. Seasons: (**a,b,c,**) NDJ, (**d,e,f**) FMA, (**g,h,i**) MJJ, and (**j,k,l**) ASO.

In the latest cross-section part, seasonal conditional extinction profiles of pure dust for three subdomains are depicted in Figure 9. *Conditional* is the term used to explain the

 doi:10.20944/preprints202203.0150.v1

incidence of dust transport cases. It is observed that November, December and January are the most stable and low intense months throughout the Eastern Mediterranean Basin. February, March and April are the dominant months for the Center and West. It can be revealed from the profiles that the incidence of dust transport events is getting higher and higher as the location shifts from west to east (avg 100 Mm^{-1}; max ~200 Mm^{-1}). Obviously, the most intense region in terms of frequency and mass is the eastern parts of Turkey and especially the Eastern Mediterranean basin. As a matter of fact, there are some low-intensity months in a year, and it would not be wrong to express Turkey, with all its regions, is under the effect of long-range transported desert originated particle load the whole year.

4. Conclusions

Turkey is located amidst North Africa, the Middle East and Asia deserts, the so-called Dusty Belt, which leads to 12-month exposure of transported particulate matter emissions. It is known that desert dust aerosols are transported within the PBL limits and low troposphere. In some cases, they may reach the free troposphere and travel further distances from the source regions. When considering Turkey's and the neighboring regions' intrinsic topographical structure and elevation characteristics, it is possible to emphasize the impact of natural barriers of mountain ranges and wet deposition dynamics of the spring and autumn months. If lofted particles overcome these high ridges or are not imposed to deposition mechanisms, they can be found at the ground level of the inner areas. This natural pollution phenomenon mainly affects the ambient air of rural and urban areas and correlatively biotic and abiotic environments. When Turkey's commitments are considered in air quality amendment actions, natural contribution to the total particulate matter load should be proofed with universal consent scientific techniques. For this purpose and to clarify the impact of natural dust phenomenon over the region, to the authors' best knowledge, 9-year 3D pure dust climatology of Turkey is formed with CALIPSO derived product for the first time. These climatology results point out horizontal and vertical distributions together with trends of Western, Central and Eastern sub-domains.

Mainly, desert dust abundancy increases in the west to east direction with prevailing and local wind systems. Moreover, synoptic-scale air movements in the region reveal seasonal variability. February is the first dust intrusion observed month, starting seasonal grouping in this study. November, December and January are the most stable and low mass-case incidence months in a year. February, March and April are the highest months for Western and Central regions. The Eastern region is the most intense in terms of frequency and mass abundance concerning the others. There is also a high season shift from spring to summer and autumn months. The seasonal grouping composed of May, June, and July months is the most active period as the whole sub-domains have the highest dust elevations, incidences, and mass loads. From inter-annual variability, oceanic oscillation systems such as ENSO, PDO and NAO are synergistically effective in the Eastern Mediterranean basin. Although all sub-domains tend to have decreased trends, the Eastern part still has the highest values close to ground level. The mountainous structure of Turkey is a natural buffer that disables particles to reach inner parts and northern latitudes. Meanwhile, it enables air quality degradation near southern slopes with downwelling accumulative effects.

To the authors' best knowledge, this study points out desert dust and total aerosol climatology for Turkey. All outputs can be used solely or as a combination of other remote sensing and in-situ techniques to better explain dust, aerosol and cloud interactions. Besides, it is thought to create a different perspective and background information for policymakers.

Preprints (www.preprints.org) | NOT PEER-REVIEWED | Posted: 10 March 2022 doi:10.20944/preprints202203.0150.v1

Author Contributions: Conceptualization, Amiridis,V., Güllü,G. and Aslanoğlu,S.Y.; methodology, Aslanoğlu,S.Y. and Proestakis,M.; software Aslanoğlu,S.Y.; validation, Aslanoğlu,S.Y. and Proestakis, M.; formal analysis, Aslanoğlu,S.Y.; investigation, Aslanoğlu,S.Y.; resources, Amiridis,V.; data curation, Aslanoğlu,S.Y., Gkikas,A.. and Proestakis, M.; writing—original draft preparation, Aslanoğlu,S.Y.; writing—review and editing, Aslanoğlu,S.Y., Güllü,G., Amiridis,V., Gkikas,A. and Proestakis,M; visualization, Aslanoğlu,S.Y.; supervision, Amiridis,V. and Güllü,G.; project administration, Aslanoğlu,S.Y.; funding acquisition, Aslanoğlu,S.Y. All authors have read and agreed to the published version of the manuscript.

Funding: The first author is funded by The Scientific and Research Council of Turkey (TUBITAK) via 2214-A International Doctoral Research Fellowship Programme, Grant agreement no: #1059B141600252.

This study is funded by Hacettepe University, Scientific Research Projects Coordination Unit, Project no: #FKA-2016-12935.

Data Availability Statement: The LIVAS database is publicly available at http://lidar.space.noa.gr:8080/livas/. LIVAS EARLINET-optimized pure-dust products are available upon request from Dr. Vassilis Amiridis (vamoir@noa.gr).

CALIPSO data provided by NASA which is obtained from the ICARE Data and Services Center online archive available at http://www.icare.univ-lille1.fr/archive (CALIPSO Science Team, 2015; ICARE Data Center, 2017)

MODIS data is publicly available at NASA Atmosphere Archive & Distribution System (LAADS) website (https://ladsweb.modaps.eosdis.nasa.gov/) via Distributed Active Archive Center (DAAC).

Acknowledgments: This publication is a part of the first author's doctoral dissertation. Special thanks to Assoc. Prof. Dr. Hatice Öncel Çekim for helping on statistical analysis.

Conflicts of Interest: The authors declare no conflict of interest. The funders had no role in the design of the study; in the collection, analyses, or interpretation of data; in the writing of the manuscript, or in the decision to publish the results.

Appendix A

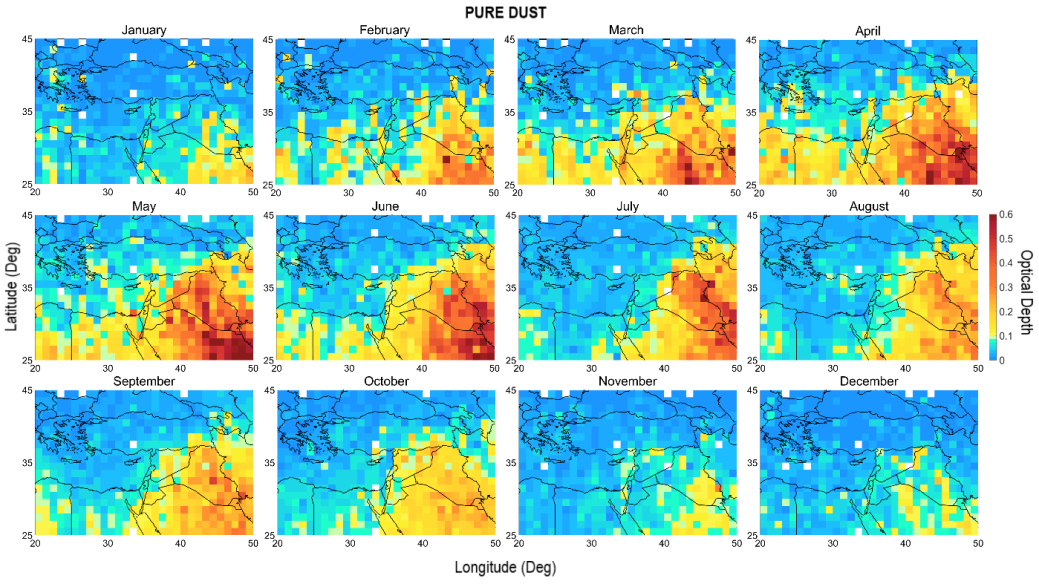

Figure A1. 9-year CALIPSO derived monthly pure dust distributions.

Preprints (www.preprints.org) | NOT PEER-REVIEWED | Posted: 10 March 2022 doi:10.20944/preprints202203.0150.v1

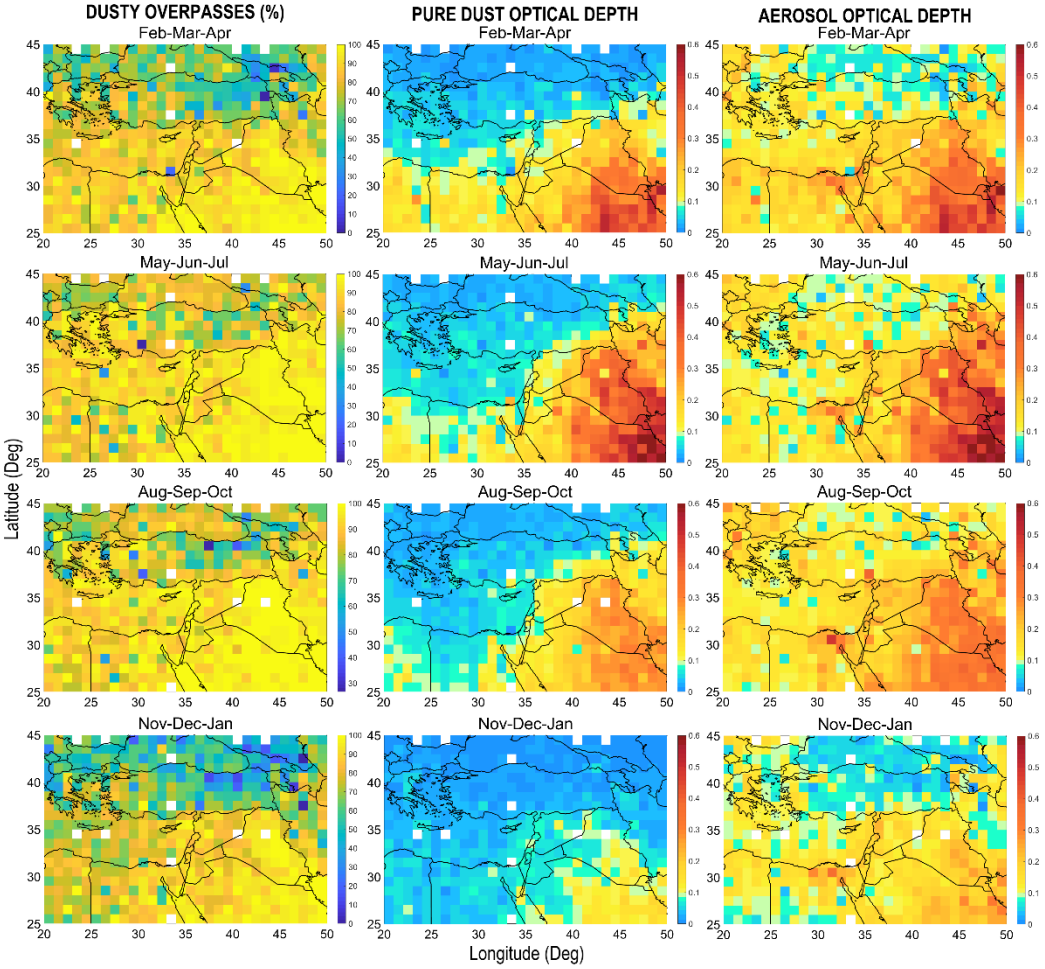

Figure A2. 9-year seasonally classified used scenes of CALIPSO dusty overpasses (%) with corresponding pure dust and total aerosol horizontal distributions.

References

1. Kim, J. J.; Smorodinsky, S.; Lipsett, M.; Singer, B. C.; Hodgson, A. T.; Ostro, B. Traffic-Related Air Pollution near Busy Roads: The East Bay Children's Respiratory Health Study. *Am. J. Respir. Crit. Care Med.* **2004**, *170* (5), 520–526. https://doi.org/10.1164/rccm.200403-281OC.
2. Filleul, L.; Rondeau, V.; Vandentorren, S.; Le Moual, N.; Cantagrel, A.; Annesi-Maesano, I.; Charpin, D.; Declercq, C.; Neukirch, F.; Paris, C.; Vervloet, D.; Brochard, P.; Tessier, J. F.; Kauffmann, F.; Baldi, I. Twenty Five Year Mortality and Air Pollution: Results from the French PAARC Survey. *Occup. Environ. Med.* **2005**, *62*, 453–460, https://doi.org/10.1136/oem.2004.014746
3. Gauderman, W. J.; Avol, E.; Lurmann, F.; Kuenzli, N.; Gilliland, F.; Peters, J.; McConnell, R. Childhood Asthma and Exposure to Traffic and Nitrogen Dioxide. *Epidemiology.* **2005**, *16*, 737–743. https://doi.org/10.1097/01.ede.0000181308.51440.75
4. Beelen, R.; Hoek, G.; van den Brandt, P. A.; Goldbohm, R. A.; Fischer, P.; Schouten, L. J.; Jerrett, M.; Hughes, E.; Armstrong, B.; Brunekreef, B. Long-Term Effects of Traffic-Related Air Pollution on Mortality in a Dutch Cohort (NLCS-AIR Study). *Environ. Health Perspect.* **2008**, *116* (2), 196–202. https://doi.org/10.1289/ehp.10767.
5. Brauer, M.; Lencar, C.; Tamburic, L.; Koehoorn, M.; Demers, P.; Karr, C. A Cohort Study of Traffic-Related Air Pollution Impacts on Birth Outcomes. *Environ. Health Perspect.* **2008**, *116* (5), 680–686. https://doi.org/10.1289/ehp.10952.
6. Querol, X.; Alastuey, a.; Pey, J.; Cusack, M.; Pérez, N.; Mihalopoulos, N.; Theodosi, C.; Gerasopoulos, E.; Kubilay, N.; Koçak, M. Variability in Regional Background Aerosols within the Mediterranean. *Atmos. Chem. Phys. Discuss.* **2009**, *9* (2), 10153–10192. https://doi.org/10.5194/acpd-9-10153-2009.
7. Stefanski, R.; Sivakumar, M. V. K. Impacts of Sand and Dust Storms on Agriculture and Potential Agricultural Applications of a SDSWS. In *WMO/GEO Expert Meeting on an International Sand and Dust Storm Warning System OP Conf. Series: Earth and Environmental Science*; 2009; *7* (1). https://doi.org/10.1088/1755-1307/7/1/012016c©2009 IOP Publishing Ltd1.
8. Giorgi, F. Climate Change Hot-Spots. *Geophys. Res. Lett.* **2006**, *33* (8), L08707. https://doi.org/10.1029/2006GL025734.
9. Giorgi, F.; Lionello, P. Climate change projections for the Mediterranean region. *Global Planet. Change*. **2008**, 200863, 90–104. doi:10.1016/j.gloplacha.2007.09.005.
10. Lelieveld, J.; Hadjinicolaou, P.; Kostopoulou, E.; Chenoweth, J.; El Maayar, M.; Giannakopoulos, C.; Hannides, C.; Lange, M. A.; Tanarhte, M.; Tyrlis, E.; Xoplaki, E. Climate change and impacts in the Eastern Mediterranean and the Middle East. *Climatic Change*. **2012**, *114*, 667–687. doi:10.1007/s10584-012-0418-4.
11. Lelieveld, J. Global Air Pollution Crossroads over the Mediterranean. *Science (80-.).* **2002**, *298* (5594), 794–799. https://doi.org/10.1126/science.1075457.
12. Griffin, D. W.; Kubilay, N.; Koçak, M.; Gray, M. A.; Borden, T. C.; Shinn, E. A. Airborne Desert Dust and Aeromicrobiology over the Turkish Mediterranean Coastline. *Atmos. Environ.* **2007**. https://doi.org/10.1016/j.atmosenv.2007.01.023.
13. Goudie, A. S. Desert Dust and Human Health Disorders. *Environ. Int.* **2013**, *63*, 101–113. https://doi.org/10.1016/j.envint.2013.10.011.
14. NA-ME-E, Northern Africa-Middle East-Europe Regional Center, Sand and Dust Storm Warning Advisory System. Available online: https://sds-was.aemet.es/ (accessed 15.05.2020).
15. CAFÉ, European Commission, DIRECTIVE 2008/50/EC OF THE EUROPEAN PARLIAMENT AND OF THE COUNCIL of 21 May 2008 on ambient air quality and cleaner air for Europe. *Off. J. Eur. Union* **2008**. https://doi.org/http://eur-lex.europa.eu/LexUriServ/LexUriServ.do?uri=OJ:L:2008:152:0001:0044:EN:PDF.
16. EEA, Particulate Matter from Natural Sources and Related Reporting under the EU Air Quality Directive, Technical Report. **2012**, *10/2012*.
17. Van Donkelaar, A.; Martin, R. V.; Brauer, M.; Kahn, R.; Levy, R.; Verduzco, C.; Villeneuve, P. J. Global Estimates of Ambient Fine Particulate Matter Concentrations from Satellite-Based Aerosol Optical Depth: Development and Application. *Environ. Health Perspect.* **2010**, *118* (6), 847–855. https://doi.org/10.1289/ehp.0901623.
18. Van Donkelaar, A.; Martin, R. V.; Brauer, M.; Boys, B. L. Use of Satellite Observations for Long-Term Exposure Assessment of Global Concentrations of Fine Particulate Matter. *Environ. Health Perspect.* **2015**, *123* (2), 135–143. https://doi.org/10.1289/ehp.1408646.
19. Vinken, G. C. M.; Boersma, K. F.; Van Donkelaar, A.; Zhang, L. Constraints on Ship NOx Emissions in Europe Using GEOS-Chem and OMI Satellite NO2 Observations. *Atmos. Chem. Phys.* **2014**, *14* (3), 1353–1369. https://doi.org/10.5194/acp-14-1353-2014.
20. Jacobson, M. Z. Global Direct Radiative Forcing Due to Multicomponent Anthropogenic and Natural Aerosols. *J. Geophys. Res. Atmos.* **2001**, *106* (D2), 1551–1568. https://doi.org/10.1029/2000JD900514.
21. Stocker, T. F.; Qin, D.; Plattner, G. K.; Tignor, M. M. B.; Allen, S. K.; Boschung, J.; Nauels, A.; Xia, Y.; Bex, V.; Midgley, P. M. *Climate Change 2013 the Physical Science Basis: Working Group I Contribution to the Fifth Assessment Report of the Intergovernmental Panel on Climate Change*; 2013. https://doi.org/10.1017/CBO9781107415324.
22. Jickells, T. D.; Baker, A. R.; Brooks, N.; Liss, P. S.; An, Z. S.; Cao, J. J.; Andersen, K. K.; Bergametti, C.; Boyd, P. W.; Hunter, K. A.; Duce, R. A.; Kawahata, H.; Kubilay, N.; LaRoche, J.; Mahowald, N.; Prospero, J. M.; Ridgwell, A. J.; Tegen, I.; Torres, R. Global Iron Connections between Desert Dust, Ocean Biogeochemistry, and Climate. *Science (80-.).* **2005**, *308* (5718), 67–71.
23. Saltzman, E. S.; Dioumaeva, I.; Finley, B. D. Glacial/Interglacial Variations in Methanesulfonate (MSA) in the Siple Dome Ice Core, West Antarctica. *Geophys. Res. Lett.* **2006**, *33* (11), 1–4. https://doi.org/10.1029/2005GL025629.
24. Rosenfeld, D.; Lohmann, U.; Raga, G.B.; O'Dowd, C.D.; Kulmala, M.; Reissell, A.; Fuzzi, S.; Andreae, M.O. Flood or Drought: How Do Aerosols Affect Precipitation? *Science.* **2008**, *321*, 1309–1313. https://doi.org/10.1126/science.1160606.

25. Ridley, D. A.; Heald, C. L.; Ford, B. North African Dust Export and Deposition: A Satellite and Model Perspective. *J. Geophys. Res. Atmos.* **2012**, *117* (2), 1–21. https://doi.org/10.1029/2011JD016794.
26. Yu, H.; Chin, M.; Yuan, T.; Bian, H.; Remer, L. a.; Prospero, J. M.; Omar, A.; Winker, D.; Yang, Y.; Zhang, Y.; Zhang, Z.; Zhao, C. The Fertilizing Role of African Dust in the Amazon Rainforest: A First Multiyear Assessment Based on CALIPSO Lidar Observations. *Geophys. Res. Lett.* **2015**, *42*, 1984–1991. https://doi.org/10.1002/2015GL063040.
27. Nickovic, S.; Vukovic, A.; Vujadinovic, M.; Djurdjevic, V.; Pejanovic, G. Technical Note: High-Resolution Mineralogical Database of Dust-Productive Soils for Atmospheric Dust Modeling. *Atmos. Chem. Phys.* **2012**, *12* (2), 845–855. https://doi.org/10.5194/acp-12-845-2012.
28. Kubilay, N.; Saydam, A. C. Trace Elements in Atmospheric Particulates over the Eastern Mediterranean; Concentrations, Sources, and Temporal Variability. *Atmos. Environ.* **1995**, *29* (17), 2289–2300. https://doi.org/10.1016/1352-2310(95)00101-4.
29. Al-Momani, I. F.; Güllü, G.; Ölmez, I.; Eler, Ü.; Örtel, E.; Sirin, G.; Tuncel, G. Chemical Composition of Eastern Mediterranean Aerosol and Precipitation: Indications of Long-Range Transport. *Pure Appl. Chem.* **1997**, *69* (1), 41–46. https://doi.org/10.1351/pac199769010041.
30. Güllü, G. H.; Ölmez, I.; Aygün, S.; Tuncel, G. Atmospheric Trace Element Concentrations over the Eastern Mediterranean Sea: Factors Affecting Temporal Variability. *J. Geophys. Res.* **1998**, *103* (D17), 21943. https://doi.org/10.1029/98JD01358.
31. Kubilay, N.; Nickovic, S.; Moulin, C.; Dulac, F. An Illustration of the Transport and Deposition of Mineral Dust onto the Eastern Mediterranean. *Atmos. Environ.* **2000**, *34* (8), 1293–1303. https://doi.org/10.1016/S1352-2310(99)00179-X.
32. Özsoy, E.; Kubilay, N.; Nickovic, S.; Moulin, C. A Hemispheric Dust Storm Affecting the Atlantic and Mediterranean in April 1994: Analyses, Modeling, Ground-Based Measurements and Satellite Observations. *J. Geophys. Res.* **2001**, *106* (D16), 18439–18460.
33. Kubilay, N.; Cokacar, T.; Oguz, T. Optical Properties of Mineral Dust Outbreaks over the Northeastern Mediterranean. *J. Geophys. Res. Atmos.* **2003**, *108* (D21), 4666. https://doi.org/10.1029/2003JD003798.
34. Holben, B. N.; Slutsker, T. I. E. I.; Tar, D.; Buis, J. P.; Setxerj, I. I. A.; Reagan, A.; J, Y.; Nakajima, T.; Lavenu, F.; Vemte, E.; Jankowiak, I.; Smirnozjt, A. AERONET-A Federated Instrument Network and Data Archive for Aerosol Characterization. *Remote Sens. Environ.* **1998**, *66* (98), 1–16.
35. AERONET, Aerosol Robotic Network. Available online: https://aeronet.gsfc.nasa.gov/ (accessed 22.01.2022).
36. Doğan, G.; Güllü, G.; Tuncel, G. Sources and Source Regions Effecting the Aerosol Composition of the Eastern Mediterranean. *Microchem. J.* **2008**, *88* (2), 142–149. https://doi.org/10.1016/j.microc.2007.11.017.
37. Gullu, G.; Olmez, I.; Tuncel, G. Source Apportionment of Trace Elements in the Eastern Mediterranean Atmosphere. *J. Radioanal. Nucl. Chem.* **2004**, *259* (1), 163–171. https://doi.org/10.1023/B:JRNC.0000015823.02927.4a.
38. Koçak, M.; Mihalopoulos, N.; Kubilay, N. Origin and Source Regions of PM10 in the Eastern Mediterranean Atmosphere. *Atmos. Res.* **2009**, *92* (4), 464–474. https://doi.org/10.1016/j.atmosres.2009.01.005.
39. Neophytou, A. M.; Yiallouros, P.; Coull, B. A.; Kleanthous, S.; Pavlou, P.; Pashiardis, S.; Dockery, D. W.; Koutrakis, P.; Laden, F. Particulate Matter Concentrations during Desert Dust Outbreaks and Daily Mortality in Nicosia, Cyprus. *J. Expo. Sci. Environ. Epidemiol.* **2013**, *23* (3), 275–280. https://doi.org/10.1038/jes.2013.10.
40. Jaafar, M.; Baalbaki, R.; Mrad, R.; Daher, N.; Shihadeh, A.; Sioutas, C.; Saliba, N. A. Dust Episodes in Beirut and Their Effect on the Chemical Composition of Coarse and Fine Particulate Matter. *Sci. Total Environ.* **2014**, *496*, 75–83. https://doi.org/10.1016/j.scitotenv.2014.07.018.
41. Tsiouri, V.; Kakosimos, K. E.; Kumar, P. Concentrations, Sources and Exposure Risks Associated with Particulate Matter in the Middle East Area—a Review. *Air Qual. Atmos. Heal.* **2015**, *8* (1), 67–80. https://doi.org/10.1007/s11869-014-0277-4.
42. Trianti, S. M.; Samoli, E.; Rodopoulou, S.; Katsouyanni, K.; Papiris, S. A.; Karakatsani, A. Desert Dust Outbreaks and Respiratory Morbidity in Athens, Greece. *Environ. Heal. A Glob. Access Sci. Source.* **2017**, *16* (1), 1–9. https://doi.org/10.1186/s12940-017-0281-x.
43. Prospero, J.M.; Lamb, P.J. African Droughts and Dust Transport to the Caribbean. *Science.* **2003,** 302 (5647) 1024–1027. https://doi.org/10.1126/science.1089915.
44. Isaelevich, P.L.; Ganor, E.; Levin, Z.; Joseph, J.H. Annual variations of physical properties of desert dust over Israel. *J. Geophys. Res. Atmos*. **2003**, 108 (D13), 4381. https://doi.org/10.1029/2002JD003163.
45. Kubilay, N.; Oguz, T.; Koçak, M.; Torres, O. Ground-Based Assessment of Total Ozone Mapping Spectrometer (TOMS) Data for Dust Transport over the Northeastern Mediterranean. *Global Biogeochem. Cycles* **2005**, *19* (1), 1–9. https://doi.org/10.1029/2004GB002370.
46. Kalivitis, N.; Gerasopoulos, E.; Vrekoussis, M.; Kouvarakis, G.; Kubilay, N.; Hatzianastassiou, N.; Vardavas, I.; Mihalopoulos, N. Dust Transport over the Eastern Mediterranean Derived from Total Ozone Mapping Spectrometer, Aerosol Robotic Network, and Surface Measurements. *J. Geophys. Res. Atmos.* **2007**, *112* (3), 1–9. https://doi.org/10.1029/2006JD007510.
47. Agacayak, T.; Kindap, T.; Unal, A.; Pozzoli, L.; Mallet, M.; Solmon, F. A Case Study for Saharan Dust Transport over Turkey via RegCM4.1 Model. *Atmos. Res.* **2015**, *153*, 392–403. https://doi.org/10.1016/j.atmosres.2014.09.012.
48. EARLINET, European Aerosol Research Lidar Network. Available online: https://www.earlinet.org/index.php?id=earlinet_homepage (accessed 11.03.2017).
49. MPLNET, The NASA Micro-Pulse Lidar Network. Available online: https://mplnet.gsfc.nasa.gov/ (accessed 12.03.2017).
50. Amiridis, V.; Balis, D. S.; Kazadzis, S.; Bais, A.; Giannakaki, E.; Papayannis, A.; Zerefos, C. Four-Year Aerosol Observations with a Raman Lidar at Thessaloniki, Greece, in the Framework of European Aerosol Research Lidar Network (EARLINET). *J. Geophys. Res. Atmos.* **2005**, *110* (21), 1–12. https://doi.org/10.1029/2005JD006190.

51. Hansell, R. A.; Liou, K. N.; Ou, S. C.; Tsay, S. C.; Ji, Q.; Reid, J. S. Remote Sensing of Mineral Dust Aerosol Using AERI during the UAE2: A Modeling and Sensitivty Study. *J. Geophys. Res. Atmos.* **2008**, *113* (18), 1–18. https://doi.org/10.1029/2008JD010246.
52. Papayannis, A.; Amiridis, V.; Mona, L.; Tsaknakis, G.; Balis, D.; Bösenberg, J.; Chaikovski, A.; De Tomasi, F.; Grigorov, I.; Mattis, I.; Mitev, V.; Müller, D.; Nickovic, S.; Pérez, C.; Pietruczuk, A.; Pisani, G.; Ravetta, F.; Rizi, V.; Sicard, M.; Trickl, T.; Wiegner, M.; Gerding, M.; Mamouri, R. E.; D'Amico, G.; Pappalardo, G. Systematic Lidar Observations of Saharan Dust over Europe in the Frame of EARLINET (2000-2002). *J. Geophys. Res. Atmos.* **2008**, *113*, D10204. https://doi.org/10.1029/2007JD009028.
53. Mona, L.; Liu, Z.; Müller, D.; Omar, A.; Papayannis, A.; Pappalardo, G.; Sugimoto, N.; Vaughan, M. Lidar Measurements for Desert Dust Characterization: An Overview. *Adv. Meteorol.* **2012**, *2012*. https://doi.org/10.1155/2012/356265.
54. Di Biagio, C.; Formenti, P.; Balkanski, Y.; Caponi, L.; Cazaunau, M.; Pangui, E.; Journet, E.; Nowak, S.; Caquineau, S.; Andreae O, M.; Kandler, K.; Saeed, T.; Piketh, S.; Seibert, D.; Williams, E.; Doussin, J. F. C. Global Scale Variability of the Mineral Dust Long-Wave Refractive Index: A New Dataset of in Situ Measurements for Climate Modeling and Remote Sensing. *Atmos. Chem. Phys.* **2017**, *17* (3), 1901–1929. https://doi.org/10.5194/acp-17-1901-2017.
55. Nisantzi, A.; Mamouri, R. E.; Ansmann, A.; Schuster, G. L.; Hadjimitsis, D. G. Middle East versus Saharan Dust Extinction-to-Backscatter Ratios. *Atmos. Chem. Phys.* **2015**, *15* (12), 7071–7084. https://doi.org/10.5194/acp-15-7071-2015.
56. Sifakis, N. I.; Iossifidis, C.; Kontoes, C. CHRISTINE Code for High ResolutIon Satellite Mapping of Optical ThIckness and ÅNgstrom Exponent. Part II: First Application to the Urban Area of Athens, Greece and Comparison to Results from Previous Contrast-Reduction Codes. *Comput. Geosci.* **2014**, *62*, 142–149. https://doi.org/10.1016/j.cageo.2013.05.011.
57. Moulin, C.; Dulac, F.; Lambert, C. E.; Chazette, P.; Jakowiak, I.; Chatenet, B.; Lavenu, F. Long-Term Daily Monitoring of Saharan Dust Load over Ocean Using Meteosat ISCCP-B2 Data. 2. Accuracy of the Method and Validation Using Sun Photometer Measurements. *J. Geophys. Res.* **1997**, *102* (D14), 16959–16969.
58. Nabat, P.; Somot, S.; Mallet, M.; Chiapello, I.; Morcrette, J. J.; Solmon, F.; Szopa, S.; Dulac, F.; Collins, W.; Ghan, S.; Horowitz, L. W.; Lamarque, J. F.; Lee, Y. H.; Naik, V.; Nagashima, T.; Shindell, D.; Skeie, R. A 4-D Climatology (1979-2009) of the Monthly Tropospheric Aerosol Optical Depth Distribution over the Mediterranean Region from a Comparative Evaluation and Blending of Remote Sensing and Model Products. *Atmos. Meas. Tech.* **2013**, *6* (5), 1287–1314. https://doi.org/10.5194/amt-6-1287-2013.
59. Hatzianastassiou, N.; Gkikas, A.; Mihalopoulos, N.; Torres, O.; Katsoulis, B. D. Natural versus Anthropogenic Aerosols in the Eastern Mediterranean Basin Derived from Multiyear TOMS and MODIS Satellite Data. *J. Geophys. Res. Atmos.* **2009**, *114* (24). https://doi.org/10.1029/2009JD011982.
60. Koren, I..; Joseph, J.H.; Israelevich, P. Detection of dust plumes and their sources in northeastern Libya. *Can. J. Remote Sens.* **2003**, *29*, 792–796. https://doi.org/10.5589/m03-036, 29 () 792.
61. Marey, H.S.; Gille, J.C.; El-Askary, H.M.; Shalaby, E.A.; El-Raey, M.E. Aerosol climatology over Nile Delta based on MODIS, MISR and OMI satellite data. *Atmos. Chem. Phys.* **2011**, *11*, 10637–10648. https://doi.org/10.5194/acp-11-10637-201.
62. Alfaro-Contreras, R.; Zhang, J.; Reid, J. S.; Christopher, S. A Study of the Longer Term Variation of Aerosol Optical Thickness and Direct Shortwave Aerosol Radiative Effect Trends Using MODIS and CERES. *Atmos. Chem. Phys. Discuss.* **2017**, 1–63. https://doi.org/10.5194/acp-2017-365.
63. Benas, N.; Beloconi, A.; Chrysoulakis, N. Estimation of Urban PM10 Concentration, Based on MODIS and MERIS/AATSR Synergistic Observations. *Atmos. Environ.* **2013**, *79*, 448–454. https://doi.org/10.1016/j.atmosenv.2013.07.012.
64. Gkikas, A.; Hatzianastassiou, N.; Mihalopoulos, N.; Torres, O. Characterization of Aerosol Episodes in the Greater Mediterranean Sea Area from Satellite Observations (2000-2007). *Atmos. Environ.* **2016**, *128*, 286–304. https://doi.org/10.1016/j.atmosenv.2015.11.056.
65. Russell, P. B.; Kacenelenbogen, M.; Livingston, J. M.; Hasekamp, O. P.; Burton, S. P.; Schuster, G. L.; Johnson, M. S.; Knobelspiesse, K. D.; Redemann, J.; Ramachandran, S.; Holben, B. A Multiparameter Aerosol Classification Method and Its Application to Retrievals from Spaceborne Polarimetry. *J. Geophys. Res. Atmos.* **2014**, *119*, 9838–9863. https://doi.org/10.1002/2013JD021411.
66. Winker, D. M.; Vaughan, M. A.; Omar, A.; Hu, Y.; Powell, K. A.; Liu, Z.; Hunt, W. H.; Young, S. A. Overview of the CALIPSO Mission and CALIOP Data Processing Algorithms. *J. Atmos. Ocean. Technol.* **2009**, *26* (11), 2310–2323. https://doi.org/10.1175/2009JTECHA1281.1.
67. Omar, A. H.; Winker, D. M.; Kittaka, C.; Vaughan, M. A.; Liu, Z.; Hu, Y.; Trepte, C. R.; Rogers, R. R.; Ferrare, R. A.; Lee, K. P.; Kuehn, R. E.; Hostetler, C. A. The CALIPSO Automated Aerosol Classification and Lidar Ratio Selection Algorithm. *J. Atmos. Ocean. Technol.* **2009**, *26* (10), 1994–2014. https://doi.org/10.1175/2009JTECHA1231.1.
68. Yorks, J. E.; McGill, M.; Rodier, S.; Vaughan, M.; Hu, Y.; Hlavka, D. Radiative Effects of African Dust and Smoke Observed from Clouds and the Earth's Radiant Energy System (CERES) and Cloud-Aerosol Lidar with Orthogonal Polarization (CALIOP) Data. *J. Geophys. Res. Atmos.* **2009**, *114* (18), 1–10. https://doi.org/10.1029/2009JD012000.
69. Kabatas, B.; Unal, A.; Pierce, R. B.; Kindap, T.; Pozzoli, L. The Contribution of Saharan Dust in PM10 Concentration Levels in Anatolian Peninsula of Turkey. *Sci. Total Environ.* **2014**, *488–489* (1), 413–421. https://doi.org/10.1016/j.scitotenv.2013.12.045.
70. Mamouri, R. E.; Ansmann, A. Estimated Desert-Dust Ice Nuclei Profiles from Polarization Lidar: Methodology and Case Studies. *Atmos. Chem. Phys.* **2015**, *15* (6), 3463–3477. https://doi.org/10.5194/acp-15-3463-2015.
71. Li, J.; Han, Z. Aerosol Vertical Distribution over East China from RIEMS-Chem Simulation in Comparison with CALIPSO Measurements. *Atmos. Environ.* **2016**, *143*, 177–189. https://doi.org/10.1016/j.atmosenv.2016.08.045.
72. Liu, D.; Wang, Z.; Liu, Z.; Winker, D.; Trepte, C. A height resolved global view of dust aerosols from the first year CALIPSO lidar measurements. *J. Geophys. Res. Atmos.* **2008**, *113* (D16), 1–15, https://doi.org/10.1029/2007JD009776.
73. Winker, D. M.; Pelon, J.; Coakley Jr., J. A.; Ackerman, S. A.; Charlson, R. J.; Colarco, P. R.; Flamant, P.; Fu, Q.; Hoff, R.; Kittaka, C.; Kubar, T. L.; LeTreut, H.; McCormick, M. P.; Megie, G.; Poole, L.; Powell, K.; Trepte, C.; Vaughan, M. A.; Wielicki, B. A. The

CALIPSO mission: A global 3D view of aerosols and clouds. *Bull. Amer. Meteor. Soc.* **2010**, *91*, 1211–1229. doi:10.1175/2010BAMS3009.1.

74. Winker, D. M.; Tackett, J. L.; Getzewich, B. J.; Liu, Z.; Vaughan, M. A.; Rogers, R. R. The Global 3-D Distribution of Tropospheric Aerosols as Characterized by CALIOP. *Atmos. Chem. Phys.* **2013**, *13* (6), 3345–3361. https://doi.org/10.5194/acp-13-3345-2013.
75. Amiridis, V.; Wandinger, U.; Marinou, E.; Giannakaki, E.; Tsekeri, A.; Basart, S.; Kazadzis, S.; Gkikas, A.; Taylor, M.; Baldasano, J.; Ansmann, A. Optimizing CALIPSO Saharan Dust Retrievals. *Atmos. Chem. Phys.* **2013**, *13* (23), 12089–12106. https://doi.org/10.5194/acp-13-12089-2013.
76. Amiridis, V.; Marinou, E.; Tsekeri, A.; Wandinger, U.; Schwarz, A.; Giannakaki, E.; Mamouri, R.; Kokkalis, P.; Binietoglou, I.; Solomos, S.; Herekakis, T.; Kazadzis, S.; Gerasopoulos, E.; Proestakis, E.; Kottas, M.; Balis, D.; Papayannis, A.; Kontoes, C.; Kourtidis, K.; Papagiannopoulos, N.; Mona, L.; Pappalardo, G.; Le Rille, O.; Ansmann, A. LIVAS: A 3-D Multi-Wavelength Aerosol/Cloud Database Based on CALIPSO and EARLINET. *Atmos. Chem. Phys.* **2015**, *15* (13), 7127–7153. https://doi.org/10.5194/acp-15-7127-2015.
77. Georgoulias, A. K.; Alexandri, G.; Kourtidis, K. A.; Lelieveld, J.; Zanis, P.; Pöschl, U.; Levy, R.; Amiridis, V.; Marinou, E.; Tsikerdekis, A. Spatiotemporal Variability and Contribution of Different Aerosol Types to the Aerosol Optical Depth over the Eastern Mediterranean. *Atmos. Chem. Phys.* **2016a**, *16* (21), 13853–13884. https://doi.org/10.5194/acp-16-13853-2016.
78. Marinou, E.; Amiridis, V.; Binietoglou, I.; Tsikerdekis, A.; Solomos, S.; Proestakis, E.; Konsta, Di.; Papagiannopoulos, N.; Tsekeri, A.; Vlastou, G.; Zanis, P.; Balis, Di.; Wandinger, U.; Ansmann, A. Three-Dimensional Evolution of Saharan Dust Transport towards Europe Based on a 9-Year EARLINET-Optimized CALIPSO Dataset. *Atmos. Chem. Phys.* **2017**, *17* (9), 5893–5919. https://doi.org/10.5194/acp-17-5893-2017.
79. Proestakis, E.; Amiridis, V.; Marinou, E.; Georgoulias, A. K.; Solomos, S.; Kazadzis, S.; Chimot, J.; Che, H.; Alexandri, G.; Binietoglou, I.; Daskalopoulou, V.; Kourtidis, K. A.; De Leeuw, G.; Van Der A, R. J. Nine-Year Spatial and Temporal Evolution of Desert Dust Aerosols over South and East Asia as Revealed by CALIOP. *Atmos. Chem. Phys.* **2018**, *18* (2), 1337–1362. https://doi.org/10.5194/acp-18-1337-2018.
80. Çiner, A. Türkiye 'nin Güncel Buzulları ve Geç Kuvaterner Buzul Çttkelİeri * Recent Glaciers and Late Quaternary Glacial Deposits of Turkey. *Geol. Bull. Turkey* **2003**, *46* (February), 55–78.
81. Koren, I.; Kaufman, Y. J.; Washington, R.; Todd, M. C.; Rudich, Y.; Martins, J. V.; Rosenfeld, D. The Bodélé Depression: A Single Spot in the Sahara That Provides Most of the Mineral Dust to the Amazon Forest. *Environ. Res. Lett.* **2006**, *1* (1). https://doi.org/10.1088/1748-9326/1/1/014005.
82. Schepanski, K.; Knippertz, P. Soudano-Saharan depressions and their importance for precipitation and dust: a new perspective on a classical synoptic concept. *Q.J.R. Meteorol. Soc.* **2011**, *137*, 1431–1445. https://doi.org/10.1002/qj.850.
83. TSI, Address based population statistics. Available online: https://data.tuik.gov.tr/Kategori/GetKategori?p=Nufus-ve-Demografi-109 (accessed 11.10.2021).
84. UNDP, World Population Prospects 2019. Available online: https://population.un.org/wpp/ (accessed 01.10.2021).
85. Farr, T. G.; Rosen, P. A.; Caro, E.; Crippen, R.; Duren, R.; Hensley, S.; Kobrick, M.; Paller, M.; Rodriguez, E.; Roth, L.; Seal, D.; Shaffer, S.; Shimada, J.; Umland, J.; Werner, M.; Oskin, M.; Burbank, D.; Alsdorf, D. The Shuttle Radar Topography Mission. *Rev. Geophys.* **2007**, *45* (1) https://doi.org/10.1029/2005RG000183.
86. Winker, D. M.; Hunt, W. H.; McGill, M. J. Initial Performance Assessment of CALIOP. *Geophys. Res. Lett.* **2007**, *34* (19), 1–5. https://doi.org/10.1029/2007GL030135.
87. Vaughan, M. A.; Powell, K. A.; Kuehn, R. E.; Young, S. A.; Winker, D. M.; Hostetler, C. A.; Hunt, W. H.; Liu, Z.; Mcgill, M. J.; Getzewich, B. J. Fully Automated Detection of Cloud and Aerosol Layers in the CALIPSO Lidar Measurements. *J. Atmos. Ocean. Technol.* **2009**, *26* (10), 2034–2050. https://doi.org/10.1175/2009JTECHA1228.1.
88. Omar, A.; Tackett, J.; Kim, M. H.; Vaughan, M.; Kar, J.; Trepte, C.; Winker, D. Enhancements to the Caliop Aerosol Subtyping and Lidar Ratio Selection Algorithms for Level II Version 4. *EPJ Web Conf.* **2018**, *176*, 2–5. https://doi.org/10.1051/epjconf/201817602006.
89. Müller, D.; Ansmann, A.; Mattis, I.; Tesche, M.; Wandinger, U.; Althausen, D.; Pisani, G. Aerosol-Type-Dependent Lidar Ratios Observed with Raman Lidar. *J. Geophys. Res. Atmos.* **2007**, *112* (16), 1–11. https://doi.org/10.1029/2006JD008292.
90. Mamouri, R. E.; Ansmann, A.; Nisantzi, A.; Kokkalis, P.; Schwarz, A.; Hadjimitsis, D. Low Arabian Dust Extinction-to-Backscatter Ratio. *Geophys. Res. Lett.* **2013**, *40* (17), 4762–4766. https://doi.org/10.1002/grl.50898.
91. Córdoba-jabonero, C.; Adame, J. A.; Campbell, J. R.; Cuevas, E.; Díaz, P.; Expósito, F.; Gil-ojeda, M. Lidar Ratio Derived for Pure Dust Aerosols : Multi-Year Micro Pulse Lidar Observations in a Saharan Dust-Influenced Region. **2016**, *23017*, 1–4. https://doi.org/10.1051/epjconf/201611923017.
92. Ricaud, P.; Sic, B.; El Amraoui, L.; Attié, J. L.; Zbinden, R.; Huszar, P.; Szopa, S.; Parmentier, J.; Jaidan, N.; Michou, M.; Abida, R.; Carminati, F.; Hauglustaine, D.; August, T.; Warner, J.; Imasu, R.; Saitoh, N.; Peuch, V. H. Impact of the Asian Monsoon Anticyclone on the Variability of Mid-to-Upper Tropospheric Methane above the Mediterranean Basin. *Atmos. Chem. Phys.* **2014**, *14* (20), 11427–11446. https://doi.org/10.5194/acp-14-11427-2014.
93. Young, S. Uncertainty Analysis for Particulate Backscatter, Extinction and Optical Depth Retrievals Reported in the CALIPSO Level 2, Version 3 Data Release. **2010**, No. 1, 3–7.
94. Georgoulias, A. K.; Alexandri, G.; Kourtidis, K. A.; Lelieveld, J.; Zanis, P.; Amiridis, V. Differences between the MODIS Collection 6 and 5.1 Aerosol Datasets over the Greater Mediterranean Region. *Atmos. Environ.* **2016b**, *147*, 310–319. https://doi.org/10.1016/j.atmosenv.2016.10.014.

95. Sayer, A. M., Munchak, L. A., Hsu, N. C., Levy, R. C., Bettenhausen, C., and Jeong, M.-J.: MODIS Collection 6 aerosol products: comparison between aqua's e-deep blue, dark target, and "merged" data sets, and usage recommendations, *J. Geophys. Res.-Atmos.* **2014**, *119*, 13965–13989, doi:10.1002/2014JD022453.
96. Cleveland, R. B; Cleveland, W. S.; McRae, J. E.; Terpenning, I. STL: A Seasonal-Trend Decomposition Procedure Based on Loess. *J. Off Stat*. **1990**, *6 (1)*, 3–73.
97. Alpert, P.; Osetinsky, I.; Ziv, B.; Shafir, H. A New Seasons Definition Based on Classified Daily Synoptic Systems: An Example for the Eastern Mediterranean. *Int. J. Climatol.* **2004**, *24* (8), 1013–1021. https://doi.org/10.1002/joc.1037.
98. Alpert, P.; Neeman, B.U.; Shay-El, Y. Intermonthly Variability of Cyclone Tracks in the Mediterranean. *J. Clim*. **1990a**, *3*, 1474. https://doi.org/10.1175/1520-0442(1990)003<1474:ivocti>2.0.co;2.
99. Alpert, P.; Abramsky, R.; Neeman, B. The prevailing summer synoptic system in Israel—Subtropical high, not Persian Trough. *Isr. J. Earth-Sciences*. **1990b,** *39*, 93.
100. Dayan, U.; Rodnizki, J. The temporal behavior of the atmospheric boundary layer in Israel. *J. Appl. Meteorol.* **1999**, *38*, 830. https://doi.org/10.1175/1520-0450(1999)038<0830:TTBOTA>2.0.CO;2.
101. Klingmüller, K.; Pozzer, A; Metzger, Swen; Stenchikov, G. L.; Lelieveld, J. Aerosol optical trend over the Middle East. *Atmos. Chem. Phys*. **2016**, *16*, 5063–5073. https://doi.org/10.5194/acp-16-5063-2016.
102. Georgoulias, A. K.; Marinou, E.; Tsekeri, A.; Proestakis, E.; Akritidis, D.; Alexandri, D.; Zanis, P.; Balis, D.; Marenco, F.; Tesche, M.; Amiridis, V. *Remote Sens.* **2020**, *12*, 1557; doi:10.3390/rs12101557.
103. Karami, S.; Hamzeh, N. H.; Alam, K.; Ranjbar, A. The study of rare frontal dust storm with snow and rain fall: Model results and ground measurements. *J. Atmos. Sol. Terr. Phys*. **2020**, *197*, 105149. https://doi.org/10.1016/j.jastp.2019.105149.
104. Cruz, J. A.; McDermott, F.; Turrero, M. J.; Edwards, R. L.; Martín-Chivelet, J. Strong links between Saharan dust fluxes, monsoon strength, and North Atlantic Climate during the last 5000 years. *Sci. Adv.* **2021**, *7*, eabe6102.
105. Dündar, C. Büyük Akdeniz Havzasında Kum ve Toz Fırtınalarının İncelenmesi ve Türkiye'yi Etkileyen Toz Kaynak Bölgelerinin Belirlenmesi, PhD Thesis, Hacettepe University Graduate School of Science and Engineering, Ankara, 2019.
106. Solomos, S.; Ansmann, A.; Mamouri, R.-E.; Binietoglou, I.; Patlakas, P.; Marinou, E.; Amiridis, V. Remote sensing and modeling analysis of the extreme dust storm hitting the Middle East and eastern Mediterranean in September 2015. *Atmos. Chem. Phys.*, **2017**, *17*, 4063–4079. https://doi.org/10.5194/acp-17-4063-2017.